

ESL-TR-91-24

**DEVELOPMENT AND TESTING OF FAST-
RESPONSE FIBER-OPTIC PRESSURE
SENSOR**

**D.B. SMITH, S.W. ALLISON, J.D. MUHS,
B.L. JOHNSON, SR.**

**APPLIED TECHNOLOGY
OAK RIDGE NATIONAL LABORATORY
POST OFFICE BOX 2003
OAK RIDGE TN 37831-7294**

DECEMBER 1996

FINAL REPORT

OCTOBER 1986 - MAY 1991

**APPROVED FOR PUBLIC RELEASE:
DISTRIBUTION UNLIMITED**

19961227 056

DTIC QUALITY INSPECTED 1



**ENGINEERING RESEARCH DIVISION
Air Force Civil Engineering Support Agency
Civil Engineering Laboratory
Tyndall Air Force Base, Florida 32403**



NOTICE

PLEASE DO NOT REQUEST COPIES OF THIS REPORT FROM HQ AFCESA/RA (AIR FORCE CIVIL ENGINEERING SUPPORT AGENCY). ADDITIONAL COPIES MAY BE PURCHASED FROM:

**NATIONAL TECHNICAL INFORMATION SERVICE
5285 PORT ROYAL ROAD
SPRINGFIELD, VIRGINIA 22161**

FEDERAL GOVERNMENT AGENCIES AND THEIR CONTRACTORS REGISTERED WITH DEFENSE TECHNICAL INFORMATION CENTER SHOULD DIRECT REQUESTS FOR COPIES OF THIS REPORT TO:

**DEFENSE TECHNICAL INFORMATION CENTER
CAMERON STATION
ALEXANDRIA, VIRGINIA 22314**

REPORT DOCUMENTATION PAGE

Form Approved

OMB No. 0704-0188

Public reporting burden for this collection of information is estimated to average 1 hour per response, including the time for reviewing instructions, searching existing data sources, gathering and maintaining the data needed, and completing and reviewing the collection of information. Send comments regarding this burden estimate or any other aspect of this collection of information, including suggestions for reducing this burden, to Washington Headquarters Services, Directorate for Information Operations and Reports, 1215 Jefferson Davis Highway, Suite 1204, Arlington, VA 22202-4302, and to the Office of Management and Budget, Paperwork Reduction Project (0704-0188), Washington, DC 20503.

1. AGENCY USE ONLY (Leave blank)		2. REPORT DATE December 1996	3. REPORT TYPE AND DATES COVERED FINAL/OCT 86 TO MAY 91	
4. TITLE AND SUBTITLE DEVELOPMENT AND TESTING OF FAST-RESPONSE FIBER-OPTIC PRESSURE SENSOR			5. FUNDING NUMBERS MIPRs N86-126 N87-96, N89-55, N90-104 AND N91-21	
6. AUTHOR(S) SMITH, D. B.; ALLISON, S. W.; MUHS, J. D.; JOHNSON, SR., B. L.			8. PERFORMING ORGANIZATION REPORT NUMBER	
7. PERFORMING ORGANIZATION NAME(S) AND ADDRESS(ES) APPLIED TECHNOLOGY OAK RIDGE NATIONAL LABORATORY POST OFFICE BOX 2003 OAK RIDGE TN 37831-7294				
9. SPONSORING/MONITORING AGENCY NAME(S) AND ADDRESS(ES) AIR FORCE CIVIL ENGINEERING SUPPORT AGENCY/RACO TYNDALL AFB FL 32403-6001			10. SPONSORING/MONITORING AGENCY REPORT NUMBER ESL-TR-91 24	
11. SUPPLEMENTARY NOTES AVAILABILITY OF THIS REPORT IS SPECIFIED ON REVERSE OF FRONT COVER.				
12a. DISTRIBUTION/AVAILABILITY STATEMENT DISTRIBUTION UNLIMITED			12b. DISTRIBUTION CODE	
13. ABSTRACT (Maximum 200 words) THIS EFFORT WAS TO DEVELOP FIBER OPTIC SENSORS FOR MEASURING RAPIDLY FLUCTUATING HIGH PRESSURES. TO UNDERSTAND THE EFFECTS OF BLAST WAVES PRODUCED BY EXPLOSIONS ON CIVIL STRUCTURES, IT IS NECESSARY TO KNOW THE STRENGTH OF SUCH PRESSURE WAVES. THE PROBLEM WITH CONVENTIONAL SENSORS WHICH USE THE MOTION OF A DIAPHRAGM OR DISK IS THAT THEY TEND TO VIBRATE ONCE THEY ARE STRUCK BY AN INITIAL PRESSURE SPIKE. THE GOAL WAS TO DEMONSTRATE FEASIBILITY OF FIBER-OPTIC SENSORS FOR PRESSURE TRANSIENT MEASUREMENT. THE SEVEN CRITERIA INVOLVED IN THE EVALUATION WERE (1) SENSITIVITY AND RANGE, (2) TIME RESPONSE, (3) NOISE CHARACTERISTICS, (4) RUGGEDNESS/DURABILITY, (5) COST OF MATERIALS AND ASSOCIATED EQUIPMENT, (6) EASE OF CONSTRUCTION, AND (7) SIMPLICITY OF SENSING MECHANISM.				
14. SUBJECT TERMS PRESSURE SENSORS, SHOCK SENSORS, OPTICAL SENSORS, FAST-RESPONSE SENSORS			15. NUMBER OF PAGES 46	
			16. PRICE CODE	
17. SECURITY CLASSIFICATION OF REPORT UNCLASSIFIED	18. SECURITY CLASSIFICATION OF THIS PAGE UNCLASSIFIED	19. SECURITY CLASSIFICATION OF ABSTRACT UNCLASSIFIED	20. LIMITATION OF ABSTRACT NONE	

EXECUTIVE SUMMARY

This is the final report of a project aimed at developing fiber-optic sensors for measuring rapidly fluctuating high pressures. To understand the effects of blast waves produced by explosions on civil structures, it is necessary to know the strength of such pressure waves. The problem with conventional sensors which use the motion of a diaphragm or disk is that they tend to vibrate once they are struck by an initial pressure spike. Therefore, the subsequent time history of the pressure impulse is masked by an oscillating signal called "ringing" that results from the vibrating diaphragm. The initial stage of this work involved evaluating, designing, and testing a number of concepts using optical fibers. The goal was to demonstrate feasibility of fiber-optic sensors for pressure transient measurement. The seven criteria involved in the evaluation were (1) sensitivity and range, (2) time response, (3) noise characteristics, (4) ruggedness/durability, (5) cost of materials and associated equipment, (6) ease of construction, and (7) simplicity of sensing mechanism. After some theoretical analysis followed by testing at static high pressures, three schemes were chosen for development and testing with high-pressure impulses. A unique shock tube facility in which to test fiber-optic sensors was then designed and fabricated. The design, operation, maintenance, and safety considerations for operating the shock tube are contained in a separate report entitled Operation, Maintenance, and Safety Manual for a Shock Tube Pressure Calibration Facility, ESL-TR-91-25. With this device, pressures as high as 24,500 kPa (3,740 psia) may be achieved in a reflected shock wave. Following construction and qualification of the shock tube fiber-optic sensor, testing commenced.

Of the sensors tested in the shock tube facility, the most promising one was based on a mechanism referred to as the "microbend" method. For this, a fiber is bent or coiled. When pressure waves impinge on the fiber, the radius of curvature changes slightly. This changes the pathways of the transmitted internal rays of light and, consequently, the transmitted intensity of light changes. This sensor was fabricated from a new fiber-optic material comprised of transparent silicone rubber. The silicone rubber fiber-optic pressure sensor (SRFOPS) exhibited the best signal-to-noise characteristics of all the sensors tested, including a conventional piezoresistive pressure transducer. No ringing was observed.

The mechanism for another sensor was based on exploiting the change of refractive index (RIFOPS-B) with pressure in the blast wave. It consisted of two conventional quartz fibers separated by a small distance and polished at a 45-degree angle so that the ends acted as internal reflecting mirrors. Light which emerges from the side of the input fiber enters the second where it is internally reflected and conveyed to a detector. A change in refractive index

which accompanies the incident shock wave bends the light in the path between the two fibers and changes the reflectivity of the fiber end mirrors. The results with this sensor configuration were poor and no further work is recommended.

A third sensor configuration was based on a combination of the above two mechanisms, microbend and refractive index change. This sensor (RIFOPS-A) was fabricated from quartz fiber and coiled in order to be sensitive to microbending. Some of the outer cladding of the coil was removed to make the transmission sensitive to index changes as well. The results were promising though signal levels and results were not as good as with the silicone rubber (SRFOPS) configuration. Nonetheless, the response was rapid and there was an absence of ringing. This configuration warrants further consideration and development.

The silicone rubber sensor (SRFOPS) may be used in liquid or gas pressure-sensing situations. The refractive-index sensor (RIFOPS-A) requires calibration in the specific medium of interest since refractive index change is a function of material. With these sensors, shock waves as high as 5,000 kPa (900 psia) were measured. Pressure profiles were obtained which clearly revealed the temporal structure of the shock waves. Pressure rise times were on the order of 100 μ s and the flow durations were on the order of 200 μ s. The measurement resolution was approximately 1,000 kPa/ μ s. No ringing was observed with any of the fiber-optic sensors. This is in contrast with a piezoresistive pressure transducer tested for comparison. The design parameters of these sensors can be easily adjusted for increased sensitivity, range, or other optimization. The shock tube calibration facility provides the means whereby to calibrate and verify the operation of each sensor prior to use in the field.

EXECUTIVE SUMMARY

- A. **OBJECTIVE:** The objective of this effort was to develop high pressure fiber-optic sensors for measuring rapidly fluctuating pressure waves. To understand the effects of blast waves produced by explosions on civil structures, it is necessary to know the strength of such pressure waves.
- B. **BACKGROUND:** Conventional sensors which use the motion of a diaphragm or disk tend to vibrate once they are struck by an initial pressure spike. Therefore, the subsequent time history of pressure impulse is masked by an oscillating signal called "ringing" that results from vibrating diaphragm.
- C. **SCOPE:** The goal was to demonstrate feasibility of fiber-optic sensors for pressure transient measurement. The seven criteria involved in the evaluation were (1) sensitivity and range, (2) time response, (3) noise characteristics, (4) ruggedness/durability, (5) cost of materials and associated equipment, (6) ease of construction, and (7) simplicity of sense mechanism. After some theoretical analysis followed by testing at static high pressures, three schemes were chosen for development testing with high-pressure impulses.
- D. **METHODOLOGY:** State of the art sensor and data system technology was applied.
- E. **TEST DESCRIPTION:** A unique shock tube facility in which to test fiber-optic sensors was designed and fabricated.
- F. **RESULTS:** The development of fast high pressure fiber-optic sensors to measure strength of explosive pressure waves.
- G. **CONCLUSIONS:** Design and fabrication specifications were provided for sensor production.
- H. **RECOMMENDATIONS:** N/A

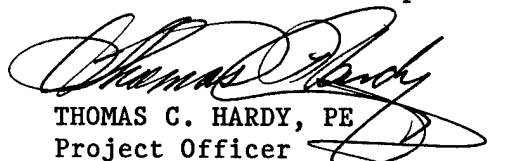
PREFACE

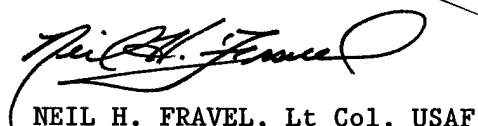
This report was prepared by Applied Technology Division, Oak Ridge National Laboratory, Oak Ridge TN 37831-7294, under MIPRs N86-126, N87-96, N98-55, N90-104 and N91-21 for the Air Force Civil Engineering Support Agency, Air Force Civil Engineering Laboratory, Tyndall Air Force Base, FL 32403-6001.

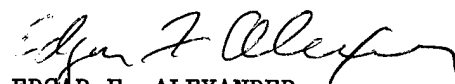
This report summarizes work done between October 1986 and May 1991. Mr Thomas Hardy was the AFCESA/RACO project officer.

This report has been reviewed by the public affairs office and is releasable to the National Technical Information Service (NTIS). At NTIS, it will be available to the general public, including foreign nations.

This technical report has been reviewed and is approved for publication.


THOMAS C. HARDY, PE
Project Officer


NEIL H. FRAVEL, Lt Col, USAF
Chief, Engineering Research
Division


EDGAR F. ALEXANDER
Chief, Air Base Operability
and Repair Branch



FRANK P. GALLAGHER III, Col, USAF
Director, Air Force Civil Engineering
Laboratory

TABLE OF CONTENTS

Section	Title	Page
I.	INTRODUCTION	1
	A. OBJECTIVE	1
	B. BACKGROUND	1
	C. SCOPE/APPROACH	1
	D. TECHNICAL ACHIEVEMENTS	2
	1. Evaluation of Sensor Concepts	2
	2. Selection and Preparation	2
	3. Shock Tube Design and Fabrication	2
	4. Testing of Sensors	2
II.	SENSOR EVALUATION	3
	A. BASIC PRINCIPLE OF FIBER-OPTIC TRANSMISSION	3
	B. TYPES OF SENSORS	3
	1. Fiber Tip Distortion	3
	2. Internal Reflection Dual Fibers	3
	3. Diaphragm	4
	4. Liquid-Core Fiber	4
	5. Coiled Fiber	4
	6. Phosphor-Tipped Fiber	5
	7. Raman Scattering	5
	C. RATIONALE FOR SELECTION	6
III.	FIBER-OPTIC PRESSURE SENSOR SYSTEM DESCRIPTION	7
	A. OVERVIEW OF SENSOR SYSTEM	7
	B. SENSOR DESIGN	7
	1. Refractive-Index-Change Fiber-Optic Pressure Sensors	7
	2. Microbend-Induced-Loss Fiber-Optic Pressure Sensors	13
	C. SENSOR SYSTEM	16
IV.	TESTING OF SELECTED FIBER-OPTIC PRESSURE SENSORS	20
	A. TEST PLAN	20
	B. SENSOR INSTRUMENTATION AND DATA PROCESSING METHODS	20
	C. STATIC TESTING	21
	D. DYNAMIC TESTING	21
	E. PERFORMANCE COMPARISON	21
V.	CONCLUSIONS AND RECOMMENDATIONS	23
	A. CONCLUSIONS	23
	B. RECOMMENDATIONS	23

TABLE OF CONTENTS
(CONCLUDED)

Section	Title	Page
REFERENCES		25
APPENDIX A.	THE SHOCK TUBE	27
APPENDIX B.	COMPUTER PROGRAM FOR CALCULATING PROPERTIES OF SHOCK WAVES	33
APPENDIX C.	TEST RESULTS	35

LIST OF FIGURES

Figure	Title	Page
1	Block Diagram of the Main Components of the Fiber-Optic Pressure Sensor System	7
2	Schematic Diagram of the Refractive-Index-Based Fiber-Optic Pressure Sensor Type A	11
3	Engineering Drawing for Shock Tube Feedthrough	12
4	Schematic Diagram of the Refractive-Index-Based Fiber-Optic Pressure Sensor Type B	14
5	Transmission Signal versus Compression of the Silicone Rubber Optical Fiber	16
6	Schematic Diagram of the Silicone Rubber Fiber-Optic Pressure Sensor	17
7	Block Diagram of the Fiber-Optic Pressure Sensor System	18
8	Electronic Schematic of the Opto-Electronic Interface Module	19
A-1	Illustration of Shock Tube Pressure Profiles before and after the Rupture of the Diaphragm	28
A-2	Shock Tube Layout Showing Positions of Instrumentation Ports 1-6	29
C-1	Calibration of (a) RIFOPS Type A and (b) SRFOPS using Static Pressures of N_2	36
C-2	Temporal Profiles of Signals Produced by (a) the SRFOPS and (b) KPPT in Response to a Shock Wave	38
C-3	Expanded Views of First Shock Wave Pulses Shown in Figure C-2(a) and C-2(b)	40
C-4	Shock Wave Profiles Shown in Figure C-3(a) and C-3(b) after Conversion into Pressure Units	41
C-5	Temporal Profiles of Signals Produced by (a) the SRFOPS and (b) the RIFOPS Type A	43
C-6	Temporal Profiles of Signals Produced by (a) the SRFOPS and (b) the RIFOPS Type B	45

LIST OF TABLES

Table	Title	Page
1	Values of the Refractive Index and Gladstone Dale Constant for Various Gases	8
A-1	Shock Tube Diaphragm-to-Port Distances	30
A-2	Values of MW and γ for Various Gases	31
C-1	FOPS Sensitivity Comparison	35

SECTION I

INTRODUCTION

A. OBJECTIVE

The objective of this research effort was to design and construct fast-response fiber-optic pressure sensors capable of measuring pressures in strong shock waves, to design and construct a shock tube suitable for testing the sensors, to test the sensors in the shock tube, and to report the results of the entire effort.

B. BACKGROUND

Pressure sensors are often used to evaluate the characteristics of shock waves produced by conventional weapons explosions. Existing shock-wave pressure sensors use piezoelectric or piezoresistive components to measure pressure; sensors based on this technology are limited in several respects. The devices (1) are subject to electromagnetic interference, (2) exhibit mechanical ringing effects, (3) are expensive, (4) often do not survive the impact of high-pressure shock waves, and (5) are unable to capture the temporal shape of shock-wave pressure transients.

Pressure sensors that employ optical fibers as their sensing elements promise to overcome all the above-mentioned limitations. Fiber-optic pressure sensors are nonelectrical, small and light, easy to install, immune to electromagnetic interference, easily integrated with data acquisition instruments, and resistant to ionizing radiation. The technology for fiber-optic pressure sensors is not fully developed, and many interesting and valuable applications are yet to be discovered and implemented.

C. SCOPE/APPROACH

The original approach of this research effort was to design, build, and test fiber-optic pressure sensors for potential use in monitoring the effects of conventional weapons explosions. Several sensing schemes were identified in the original statement of work as promising approaches. The initial effort showed sufficient potential so that the objective was expanded to include (1) static high-pressure testing and (2) design and fabrication of a facility for generating reproducible high-pressure waves similar to those of the envisioned application. That facility consisted of a shock tube and a supporting gas-handling manifold. The final objective was to test and evaluate three of the most promising fiber-optic sensors in the shock tube.

D. TECHNICAL ACHIEVEMENTS

1. Evaluation of Sensor Concepts

Evaluations and experiments were conducted on the sensor concepts. The effort included determining sensitivities. The effort showed sufficient promise on this phase of the project to make continuation of the work worthwhile. This work was reported in Reference 1. A summary is included in the next section. Near the end of this effort, preparations were made for a field test at Tyndall Air Force Base. After onsite consultations, a decision to pursue shock tube testing, as an alternative, was made.

2. Selection and Preparation

Evaluations continued for the purpose of selecting the three most promising gauges and preparations were made for shock tube testing. The original plans were to use a surplus shock tube from a closed-out U.S. Government Project. Upon delivery, it was determined that the surplus shock tube was not suitable for attaining sufficiently high pressures for realistic evaluations and would require additional machining and decontamination. It was determined that a new shock tube, designed and optimized for this application, would be more cost-effective than modification and decontamination of the old one. Sensor testing with static high pressures was performed. Several fiber sensors were found sensitive to blast waves from fireworks but the results underscored the fact that there was a need to be able to generate reproducible pressure waves of known or verifiable strength. The theory of shock tube operation showed that this could be done and provided the initial results on which to base a plan for testing fiber-optic pressure sensors. Reference 2 is a summary of this effort.

3. Shock Tube Design and Fabrication

This stage of the project was primarily concerned with the design and fabrication of the shock tube. Actual costs of the design, fabrication, and component costs exceeded design estimates. This delayed safety qualification, testing of the shock tube operation, and dynamic testing of the chosen sensors.

4. Testing of Sensors

This stage provided for final testing of three chosen sensors and this final report. Upon completion of test work, the shock tube system was turned over to Air Force Engineering Services Center personnel, along with prototype sensors, support equipment, and spares. A set of blueprints and a shock tube operation manual were also provided.

SECTION II

SENSOR EVALUATION

A. BASIC PRINCIPLE OF FIBER-OPTIC TRANSMISSION

The principle on which fiber optics is based is called total internal reflection. When a ray of light is incident at a boundary between two transparent media, 100 percent reflection is possible under the following conditions: the ray of light must be propagating in the higher-refractive-index medium. If the angle of incidence is sufficiently small, total internal reflection will occur. This mechanism has made it possible to transmit light many kilometers via optical fibers. If the fiber is perturbed in any way, some fraction of light that would have been reflected no longer satisfies the above condition and escapes from the fiber core, resulting in a change in signal received by a detector. This is the basis for the field of fiber-optic sensing.

B. TYPES OF SENSORS

A variety of sensors were evaluated. The initial scope of the work called for investigations into fiber tip distortion, light leakage, diaphragm, lever, liquid-core, coiled fiber, and phosphor-tipped fiber. These, as well as others, were considered and evaluated. Reference 1 describes the results of some of these evaluations through calendar year 1987. There has been much development in fiber-optic sensing during the course of this work and the evidence is that this will continue. Consequently, effort has always been made to keep up with these developments for possible application to transient high-pressure testing. The following is a summary of all previous work.

1. Fiber Tip Distortion

There were two embodiments of this concept. In the first, a single optical fiber was stripped of cladding at the sensing end and coated with aluminum. Distortion of the fiber tip produces change in light intensity reflected internally. This method appeared to work in the lab. Difficulties associated involved separating signal change from noise disturbances at other points along the fiber and keeping the aluminum film on the sensor. A second embodiment of this approach utilized a transparent optical ball placed at the end of the fiber, with a mechanical cylindrical plunger on top of the ball to transmit the force. Some mechanical tests illustrated usable signal change but there was considerable fabrication difficulty.

2. Internal Reflection Dual Fibers

This was a combination of the light leakage and lever concepts. It primarily uses a leakage of light transmission due to

refractive-index changes and an optical lever effect. Two fibers are polished at a 45-degree angle and placed side by side. Light rays conveyed by one fiber are internally reflected from this into the other receiving fiber where another internal 45-degree reflection directs the light down the receiving fiber to a detector. Changes in the index of refraction, which accompany high-pressure pulses, change the reflectivity at each interface. Distortions of the fiber can also change the angle, hence an optical lever effect can also occur. This approach was chosen for testing in the shock tube and will be described in greater detail in Section III.B.1.

3. Diaphragm

This approach, possibly the most commonly used fiber-optic pressure-sensing method, uses two fibers placed side by side. Light emerging from a delivery fiber is reflected from a circular diaphragm into a receiving fiber. The diaphragm flexes as a result of pressure impulses. This causes more or less light to be directed to the receiving fiber. As with the typical piezoelectric-based transducer, this method is susceptible to ringing. This was observed when testing with M-80 fireworks.

4. Liquid-Core Fiber

Liquid-core fibers consisting of hollow glass or quartz tubing filled with a higher-refractive-index liquid can transmit light efficiently. The transmission of liquid-core fiber is very sensitive to vibration and acoustic impulses. This approach suffered from fabrication difficulty, complexity of the sensing mechanism, and analytical modeling.

5. Coiled Fiber

For this, a single optical fiber is formed into a bend or coil. Some of the cladding is removed so that the air or other external medium is in intimate contact with the fiber core. Two mechanisms can produce changes in the signal transmitted by the fiber. Impulse pressure can change the shape of the bends of the coil and thereby deflect the light guided by the fiber. In addition, high-pressure air is characterized by a change in the index of refraction. An increase in index will cause more light to leak or escape the fiber core. Several embodiments were evaluated. Two of these were selected for subsequent shock tube testing and are described in more detail later in this report. The first is referred to as Refractive Index Fiber-Optic Pressure Sensor Type B (RIFOPS-B). A new type of optical fiber material recently became available. It is made from transparent silicone rubber. It is referred to as the Silicone Rubber Fiber-Optic Pressure Sensor (SRFOPS).

6. Phosphor-Tipped Fiber

Fiber-optic-based phosphor thermometry is an established method for a variety of difficult-to-access measurement situations. Extension of the method for pressure sensing was considered. The intensity and duration of fluorescence of phosphors induced by a short pulsed laser are known to be pressure-dependent. This dependence begins at about 69,000 kPa (10,000 psi). Thus, a means to mechanically amplify pressure by a factor of 10 is needed. One disadvantage noted in testing with mechanically applied pressure was the formation of color centers. These indicate some possibly irreversible physical changes in the compression properties, thus some irreversible physical change in the material. Nonetheless, the method still appears promising for further scientific investigations. This technique was initially chosen as one of the three to be tested in the shock tube. It was supplanted by the silicone rubber fiber coil method.

7. Raman Scattering

An extrinsic fiber sensor based on Raman scattering from N_2 molecules in air was investigated. Calculations showed that air pressure measurements were feasible, albeit three expensive components would be required: a laser, a high-stray-light rejection monochromator, and a photomultiplier tube detector.

Fiber-optic pressure sensors are usually grouped into two categories: those in which pressure-induced perturbations result in a modulation of the intensity of transmitted light and those in which the perturbations result in a modulation of the phase of the transmitted light. In intensity-modulation sensors, pressure is measured by correlating transmission characteristics with external pressures. All the sensors mentioned above are intensity-modulation sensors. In phase-modulation sensors, pressure is measured by observing the constructive or destructive interference effects produced by changes in external pressure. Phase modulation schemes usually employ a single-mode fiber and an interferometric means for modulating the phase. Therefore, these sensors have excellent sensitivity and accuracy, but they require more signal processing, are difficult to align, and are more expensive and fragile than intensity-modulated sensors.

Intensity-modulation sensors are fairly simple in construction and can be implemented with multimode optical fibers, but have less dynamic range than phase-modulation sensors and have therefore received essentially all of the consideration for this project. The sensitivity and accuracy provided by phase-modulation sensors is not required for shock-wave applications, and these qualities can be traded off for the advantages provided by intensity-modulation sensors. Phase-modulation sensors were thus considered; however, based on these considerations, the testing effort focused exclusively on the intensity-modulated sensors described in this report.

C. RATIONALE FOR SELECTION

One criterion must be met if a fiber-optic pressure sensor is to be used in explosion environment testing. This is that the proposed fiber-optic sensor must have the potential to have advantages over the commonly used diaphragm sensor. In order to answer in the affirmative for a given sensor, its characteristics in seven categories must be evaluated.

1. Sensitivity and range. Sensitivity and range are considered together. Many types of fiber-optic pressure sensors reported in the literature are quite sensitive but are designed for lower pressures.
2. Time response. The sensor must be able to respond to pressure impulses and not exhibit ringing which characterizes the diaphragm-based approaches.
3. Noise characteristics. The major reason for the choice of the type sensors studied was the expectation of significant improvement in noise characteristics in field use. This is related to the previous criterion: ringing is one of the undesirable noise sources.
4. Ruggedness/durability. To be of use, the sensor must be able to survive long enough to transmit the information.
5. Cost of materials and associated equipment. This requirement eliminates laser-spectroscopy-based techniques such as Raman scattering due to expense of lasers, detection, and analysis equipment.
6. Ease of construction. While the materials expense of some schemes was relatively small, the labor cost of construction was found to be a disadvantage.
7. Simplicity of sensing mechanism. Experience teaches that simpler devices have fewer problems and complications.

Three schemes were chosen for final testing in the shock tube. The first was a two-fiber, refractive-index-based configuration called RIFOPS-A. The second, RIFOPS-B, was a coiled sensor based both on microbending and index of refraction. The third sensor, SRFOPS, was a coiled silicone rubber fiber based on the microbend concept. All of these were inexpensive in terms of cost of materials and ease of construction. For the refractive-index sensors, the nature of the sensing mechanism, as will be discussed below, dictates a near-instantaneous response to pressure changes and an absence of ringing. Static testing indicated the potential sensitivity and range of all three sensors. From the discussion of the other sensing schemes discussed above, it should be clear that these were the best candidates for initial shock tube testing.

SECTION III

FIBER-OPTIC PRESSURE SENSOR SYSTEM DESCRIPTION

A. OVERVIEW OF SENSOR SYSTEM

The sensor system consists of three main components: a fiber-optic pressure sensor (FOPS), an opto-electronic interface (OEI) module, and a digital voltmeter or digitizing oscilloscope to record the output of the OEI. A voltmeter is sufficient for measuring static pressures, while an oscilloscope is required for measuring rapidly changing pressures. A block diagram of the sensor system is shown in Figure 1.

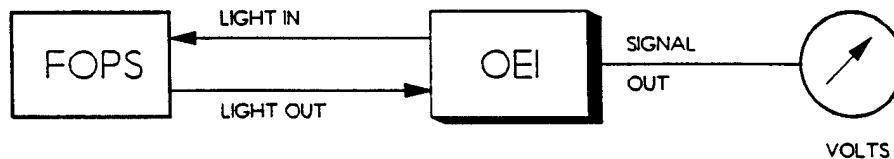


Figure 1. Block Diagram of the Main Components of the Fiber-Optic Pressure Sensor System.

Light from a light-emitting diode (LED) in the OEI is sent to the FOPS through an input optical fiber, is transmitted through the FOPS, and is returned to a photodiode detector in the OEI through an output fiber. The amplified output of the detector is transmitted to the voltmeter or oscilloscope with a 50-ohm coaxial cable. The OEI output signal is a function of the pressure sensed by the FOPS.

The design and fabrication of the three FOPS selected for shock tube testing and the instrumentation setup for shock tube testing of the FOPS are described below.

B. SENSOR DESIGN

1. Refractive-Index-Change Fiber-Optic Pressure Sensors

a. Sensing Mechanism

For light with wavelength λ propagating in a gaseous medium, the refractive index n is related to the gas density ρ by (Reference 3),

$$n_{\lambda} = 1 + K\rho . \quad (1)$$

K is known as the Gladstone Dale constant. Since gas density

varies with pressure,* n_λ is a function of the pressure in the gas. Equation (1) shows that n increases linearly with ρ at a rate K i.e.,

$$\Delta n_\lambda / \Delta \rho = K . \quad (2)$$

Table 1 lists standard handbook values of n and K for various gases.

TABLE 1. VALUES OF THE REFRACTIVE INDEX AND GLADSTONE DALE CONSTANT FOR VARIOUS GASES.

Gas	n (at STP and $\lambda=590$ nm)	K (m^3/kg)
Air	1.000292	226×10^{-6}
N_2	1.000297	237×10^{-6}
He	1.000035	197×10^{-6}
Ne	1.000067	74×10^{-6}
Ar	1.000284	159×10^{-6}

A simple calculation can be done to estimate the change produced in n by a fifty-fold increase in the density of air at atmospheric pressure. From Equations (1) and (2) and the data in Table 1, we have

$$\begin{aligned} \Delta n_{(n-1)} &= K \Delta \rho = K(50\rho - \rho) = K(49\rho) = K[49(n-1)/K] = 49 \\ &= 49(0.000292) \\ &= 0.0143 . \end{aligned} \quad (3)$$

*The equation of state of a real gas can be expressed in the form

$$p = A\rho + B\rho^2 + C\rho^3 + \dots ,$$

where the virial coefficients A , B , C , etc., are functions of the gas constant R and the absolute temperature T . For an "ideal" gas $A = RT$ all other coefficients are zero, and the equation of state is

$$p = \rho RT .$$

Therefore, the density of an ideal gas is proportional to its pressure and inversely proportional to its temperature.

Hence, the index of refraction changes from 1.000292 to 1.014600, an increase of 1.4 percent.

An optical fiber can be used to sense changes in n produced by changes in pressure. In a step index optical fiber, the total number N of propagational modes of light that are transmitted in the fiber core is given by (Reference 4)

$$N = \frac{1}{2} \left(\frac{2\pi r}{\lambda} \right)^2 \sqrt{n_{\text{core}}^2 - n_{\text{clad}}^2}, \quad (4)$$

where r is the radius of fiber core, λ is the wavelength of the transmitted light, and n_{core} and n_{clad} are the refractive indices of the fiber core and fiber cladding, respectively. The intensity of the light transmitted by the fiber is a function of N .

When the cladding is removed from a fiber core, the medium surrounding the core becomes the new cladding and N will be determined by the n of the medium. Thus, the intensity of the light transmitted by the fiber will be modulated by pressure changes in the medium. Furthermore, the pressure sensitivity $\Delta N/\Delta p$ of the fiber will be proportional to the amount of cladding removed and replaced by the surrounding medium.

Equations (3) and (4) can be used to estimate the change in N produced by a fifty-fold increase in the density of air surrounding a 1000- μm -diameter silica glass fiber ($n_{\text{core}} = 1.457$) that is fully filled by a light source having $\lambda = 590$ nm. (A fifty-fold increase in density corresponds to a fifty-fold increase in pressure, assuming the gas in the medium is an ideal gas and that the temperature remains constant during the increase.) We have

$$\frac{\Delta N}{N} = \frac{\sqrt{n_{\text{core}}^2 - n_{\text{clad}}'^2} - \sqrt{n_{\text{core}}^2 - n_{\text{clad}}^2}}{\sqrt{n_{\text{core}}^2 - n_{\text{clad}}^2}} = -0.013, \quad (5)$$

where $n_{\text{clad}} = 1.000292$ is the index of refraction of the gas before the density change, and $n_{\text{clad}}' = 1.014600$ is the index of refraction of the gas after the density change. Hence, a fifty-fold increase in gas density would produce a 1.3 percent decrease in transmitted modes.

The refractive index change sensing mechanism has two disadvantages that must be addressed. First, changes in n are produced by temperature changes as well as pressure changes. This means that if a temperature change accompanies a pressure change, it might be very difficult to separate the pressure-induced change in N from the temperature-induced change in N . Second, the sensor must be calibrated for each gas medium in which it is used, since the values of n and K vary with the particular gas medium. (The calibration procedure is described in Section A of Appendix C.)

b. Sensor Fabrication

(1) Refractive Index Fiber-Optic Pressure Sensor Type A (RIFOPS-A)

A schematic diagram of refractive index design type A is shown in Figure 2. A shock tube feedthrough (Figure 3) was used as the sensor mount. Light from an LED source is input to the sensor through one fiber and is output through the other. The input and output fibers are both 1000- μ m-diameter core silica multimode fibers. One end of each fiber was cleaved and polished flat, while the other end was cleaved and polished at an angle of 45 degrees. The fibers were cleaved by scoring them with a glass microscope slide, then gently bending them at the scored line until a smooth break was obtained. An abrasive paper with a Number 600 or finer grit is sufficient for polishing the ends of the fibers.

Approximately 3 mm of cladding (buffer) was removed from the ends with the 45-degree interface. The cladding was removed with the use of hydrofluoric acid. Epoxy cement (Devcon® 14250) was used to pot the fibers into the sensor mount (shock tube feedthrough). The fiber axes are parallel and there is a gap of about 0.5 mm between their outside diameters. The size of the gap determines the sensitivity of the sensor and the value of its signal-to-noise ratio: the larger the gap, the better the sensitivity and the worse the signal-to-noise ratio.

A large fraction of the light from the input fiber is reflected from its end and is transmitted through the surrounding medium to the end of the other fiber, where a fraction is again reflected at the end and is then transmitted into the output fiber. The intensity of the transmitted light depends on the value of n at the 45-degree interfaces; n increases as the pressure in the medium increases, and the light reflected at the interfaces decreases.

This sensor design provides several advantages. First, the sensing mechanism provides the sensor with a virtually instantaneous response to changes in pressure. Second, the sensing region is very small, allowing the sensor to be located in an unobtrusive manner. Third, since the sensor has no moving parts and is firmly fixed in the sensor mount (shock tube feedthrough), it requires no adjustments after fabrication.

The primary disadvantage of this sensor design is that care must be taken during its fabrication to ensure that light will be efficiently coupled between the fibers. The maximum amount of light is internally reflected at the 45-degree interfaces when the surfaces are carefully polished. A low-power (50X) microscope was useful for examining these surfaces during the polishing procedure. Furthermore, the fibers can be best aligned in the feedthrough by launching a bright light source into one fiber, then aligning the fibers until the maximum emission is observed from the other fiber.

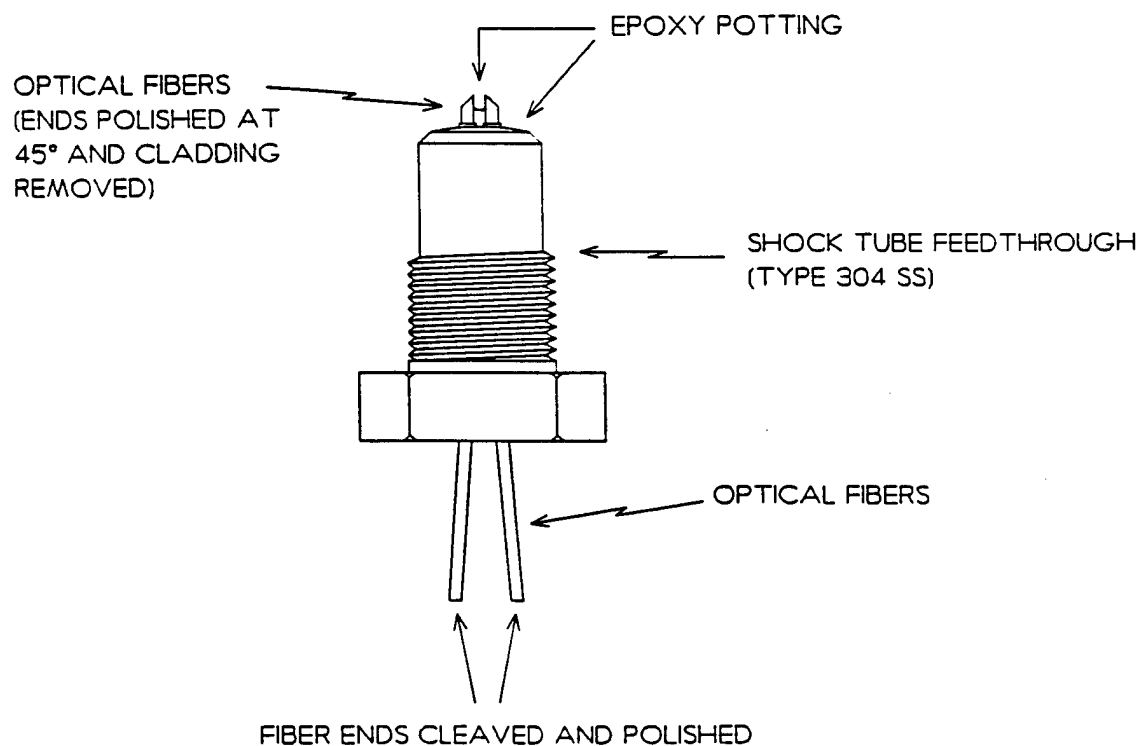


Figure 2. Schematic Diagram of the Refractive-Index-Based Fiber-Optic Pressure Sensor Type A (RIFOPS-A). Details of its fabrication are given in the text.

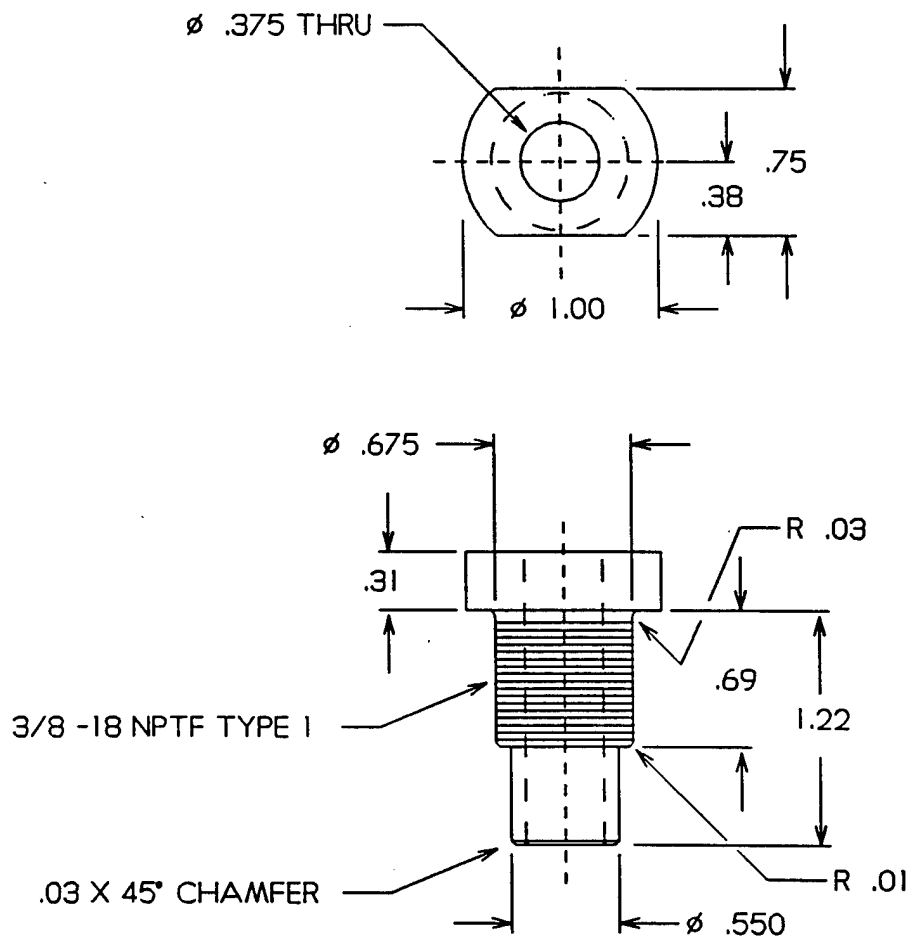


Figure 3. Engineering Drawing for Shock Tube Feedthrough.
 All dimensions are in inches. Fiber-optic pressure
 sensors are mounted in feedthroughs for shock
 testing.

(2) Refractive Index Fiber-Optic Pressure Sensor Type B (RIFOPS-B)

The second design for a refractive-index-based pressure sensor is shown in Figure 4. This approach was previously reported in Reference 2. A standard plastic-clad silica-based glass fiber (Ensign Bickford) having a 600- μm -diameter core is implemented as the sensing element. The cladding and buffer were stripped from a 2.5-cm-long segment of a 1-meter-long fiber with the use of hydrofluoric acid. The 2.5-cm-long segment of bare core is the sensing region. The length of this segment determines the sensitivity of the sensor and the value of its signal-to-noise ratio: the longer the segment, the larger the sensitivity and the smaller the signal-to-noise ratio.

A 180-degree bend was formed in the fiber by heating the segment with a microtorch. The bend has a radius of 1 cm, and the fiber is potted into the sensor mount with epoxy cement (Devcon® 14250) so the bend extends about 5 mm beyond the end of the mount. The magnitude of the bend radius was small enough to allow the fiber to fit inside a shock tube feedthrough (Figure 3), but was not so small as to excessively diminish the signal-to-noise ratio of the transmitted signal. It is extremely difficult, if not impossible, to bend fibers with core diameters larger than 600 μm in a radius this small.

The primary advantages of this sensor design is that it is inexpensive and easy to fabricate. The primary disadvantage is that the sensing region is more fragile than ordinary fiber, since its cladding has been removed and has been heat treated. Care must be taken to ensure that the sensing region does not collide with hard or sharp surfaces.

2. Microbend-Induced-Loss Fiber-Optic Pressure Sensors

a. Sensing Mechanism

The second sensing technique is based on the concept of microbending (Reference 5). All optical fibers radiate energy when bent, and the highest-order transmission modes are the most likely to be radiated at the location of the bend. If the bending of the fiber is in response to a change in the pressure of the medium surrounding the fiber, the change in the intensity of transmitted light can be correlated to change in pressure. As the pressure increases, the fiber's cross section is compressed and the intensity of transmitted light is decreased.

The usual implementation of this technique is to compress a silica-based glass fiber between two corrugated plates (Reference 6). When the fiber is compressed, the plates create "microbends" in the fiber. This sensing technique provides very good sensitivity to pressure changes produced by acoustic waves, where pressure variations are on the order of 10^{-6} pascal, but does not provide a dynamic range sufficient for measurements in high-

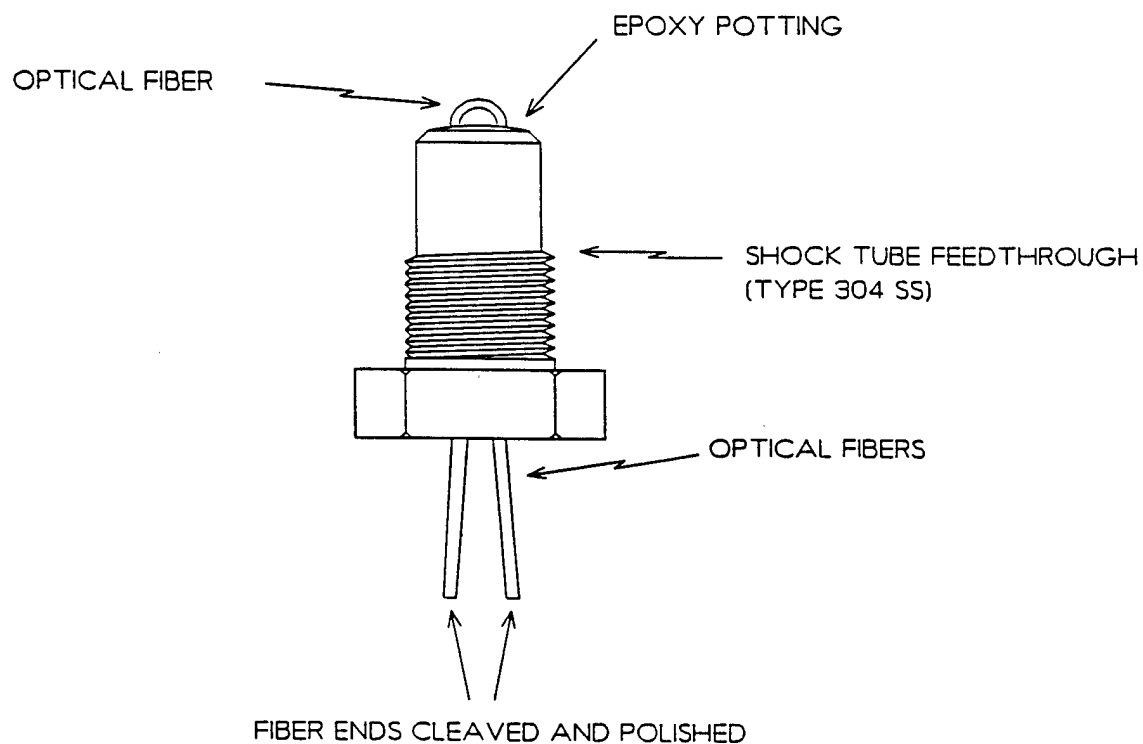


Figure 4. Schematic Diagram of the Refractive-Index-Based Fiber-Optic Pressure Sensor Type B (RIFOPS-B). Details of its fabrication are given in the text.

pressure shock waves, where pressure variations are on the order of 10^6 pascal.

A silicone rubber optical fiber* is well-suited for microbending without corrugated plates. The elastic behavior of the fiber provides it with a large dynamic range and allows it to be substantially compressed without damage. Pressures on the order of those can compress the fiber's cross section.

The effect of compression on the transmission signal ($\lambda = 660$ nm) of a silicone rubber optical fiber is shown in Figure 5. The transmission signal was measured as a 3.8-mm-long segment at the middle of a 2-meter-long fiber and was uniformly compressed between two parallel surfaces. The decrease in fiber diameter was measured along the compression axis. The maximum compression shown in the figure (21.5 percent) was produced by a pressure of approximately 2,000 kPa.

b. Sensor Fabrication

A schematic diagram of the silicone rubber fiber-optic pressure sensor (SRFOPS) design is shown in Figure 6. A shock tube feedthrough (Figure 3) was used as the sensor mount. Light from an LED source is input to the sensor through one end of the fiber and is output through the other end. The fiber has a core diameter of 1.7 mm, a cladding diameter of 3.2 mm, and is surrounded by an opaque (black) sheathing. The fiber may be cleaved satisfactorily with a razor blade.

The fiber is bent at a radius of about 3 mm, and the bend extends about one fiber diameter beyond the end of the shock tube feedthrough. The smaller the bend radius, the smaller the sensor's signal-to-noise ratio.

The fiber is potted into the feedthrough with epoxy cement, so that the pressure-sensing region consists of only the top half of the bent fiber (i.e., about 50 percent of the outer surface will be exposed to changes in external pressure). The sensitivity of the sensor is determined by the size of the sensing region; the greater the sensing region, the greater the sensitivity.

The primary advantages of this sensor design are that it is very inexpensive to fabricate and is extremely rugged. Its primary disadvantage is that the fiber core, cladding, and sheathing are viscoelastic materials, and as such they may exhibit

*The distributor for the silicone rubber optical fiber is Bridgestone Engineered Products Corporation, 955 Dairy Ashford, Suite 226, Houston, Texas 77079. The part number is OS101.

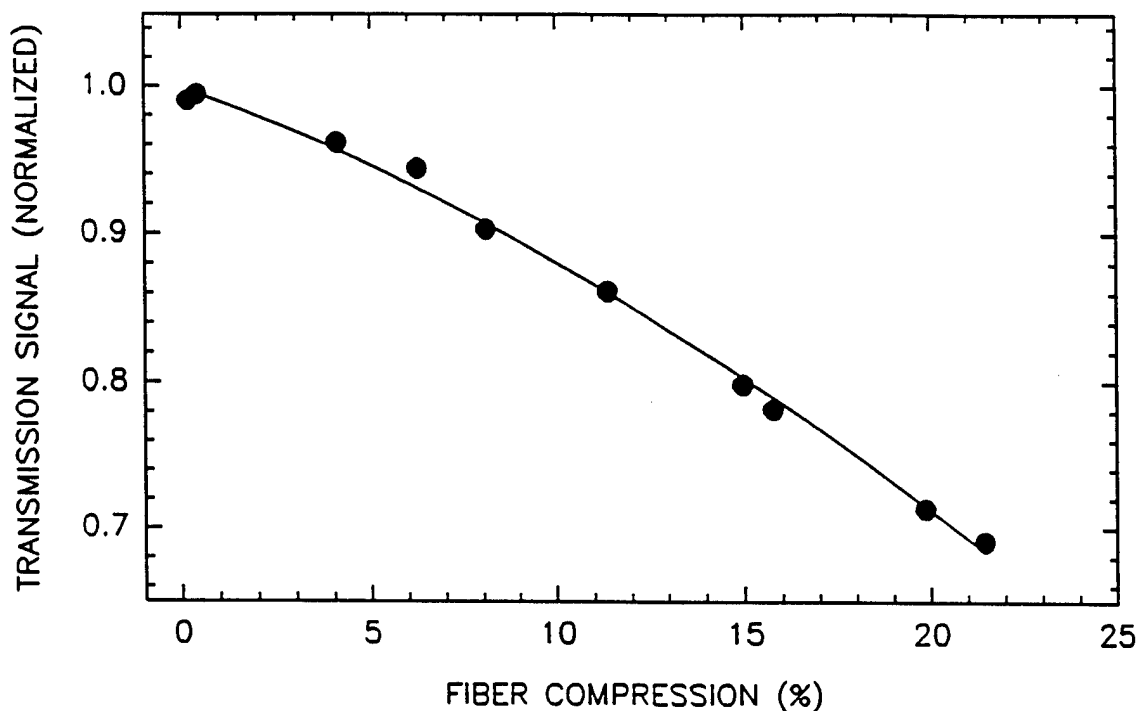


Figure 5. Transmission Signal versus Compression (Percent Decrease in Fiber Diameter) of the Silicone Rubber Optical Fiber. The line represents a second-order polynomial fit to the data.

a nonlinear response to the rate of compression (i.e., pressure) loading.

C. SENSOR SYSTEM

The components required for shock tube testing of the fiber-optic pressure sensor test system are the sensor, the OEI module, a digitizing oscilloscope, and a laboratory microcomputer. These components and their interconnections are shown in Figure 7.

The OEI module (Figure 8) contains two LED sources [red ($\lambda = 663$ nm) and infrared ($\lambda = 821$ nm)], a photodiode detector, and a linear-gain signal preamplifier. The LED output and photodiode input on the OEI are coupled to the input and output fibers of the FOPS with standard AMP multimode optical-fiber couplers. The OEI output is transmitted to the oscilloscope with the use of a 50-ohm coaxial cable. Waveforms are stored on the disk of a laboratory microcomputer by transferring the waveform via an IEEE-488 interface between the two devices.

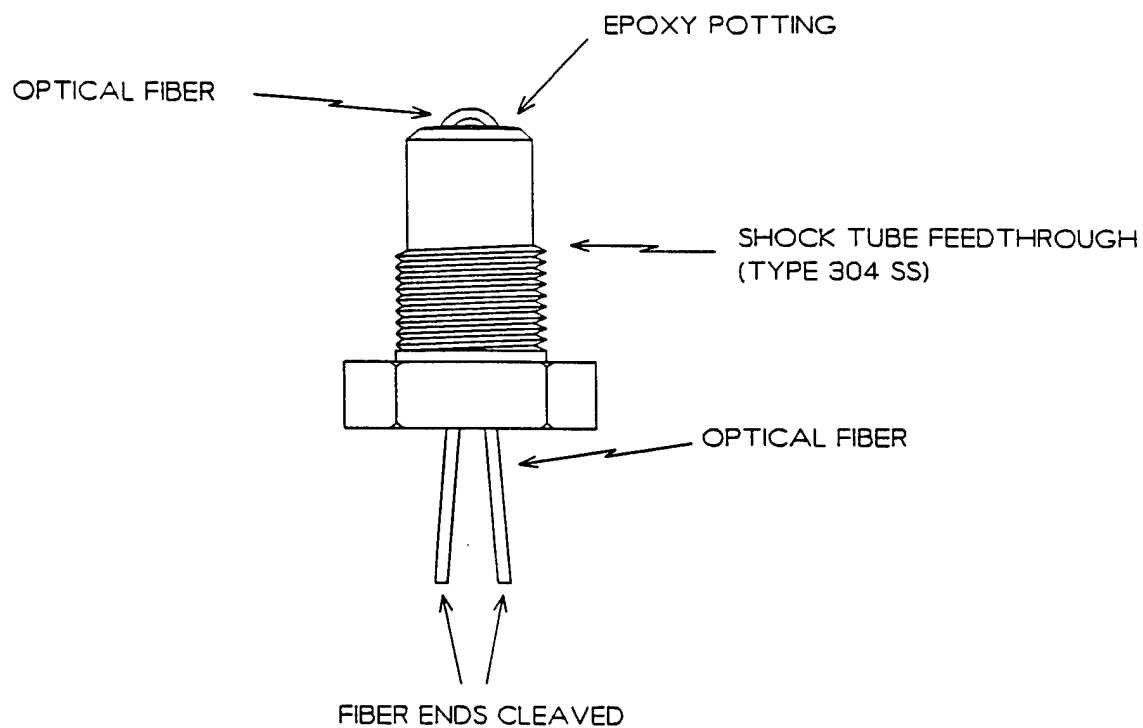


Figure 6. Schematic Diagram of the Silicone Rubber Fiber-Optic Pressure Sensor (SRFOPS). Details of its construction are given in the text.

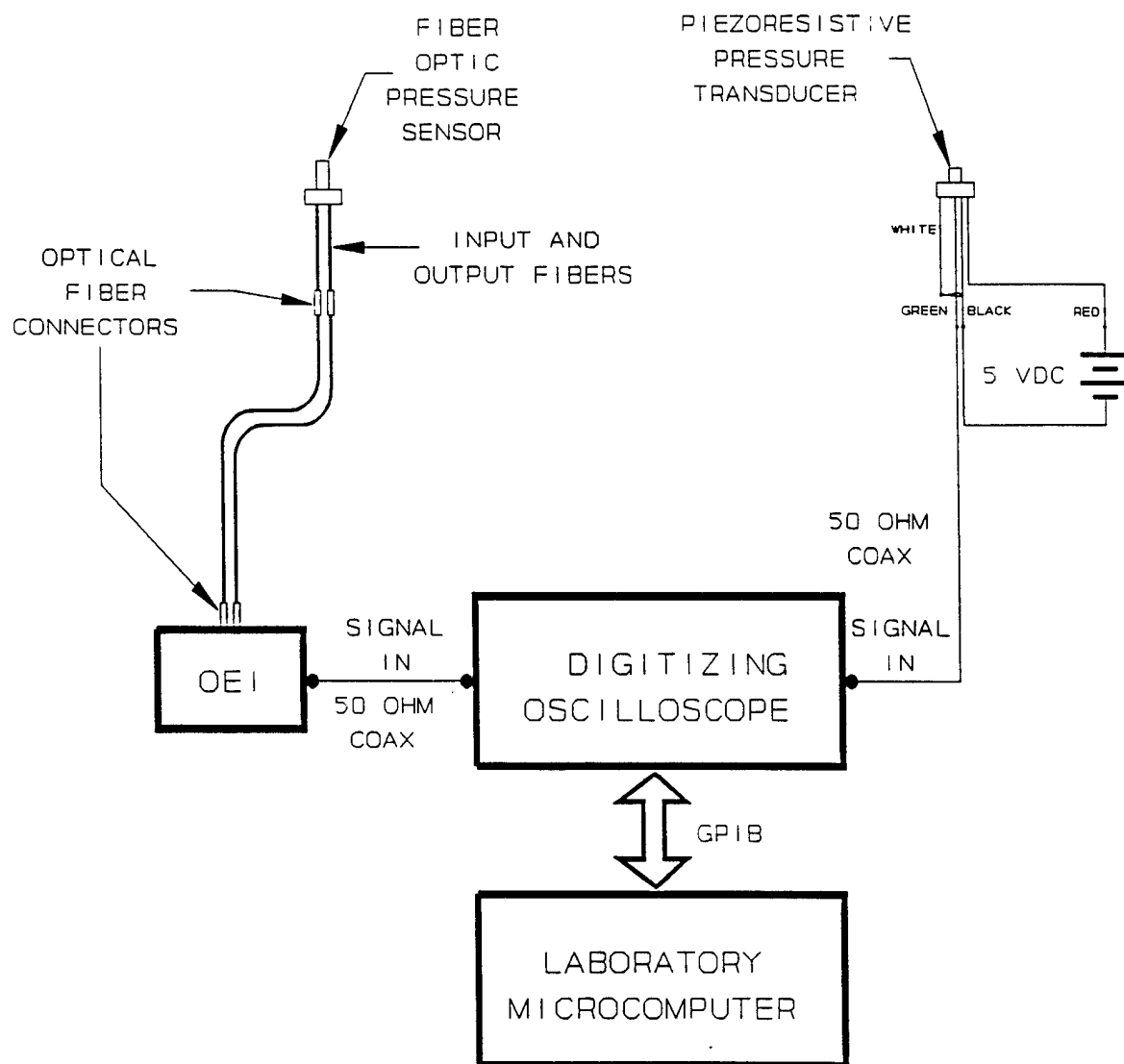


Figure 7. Block Diagram of the Fiber-Optic Pressure Sensor System.

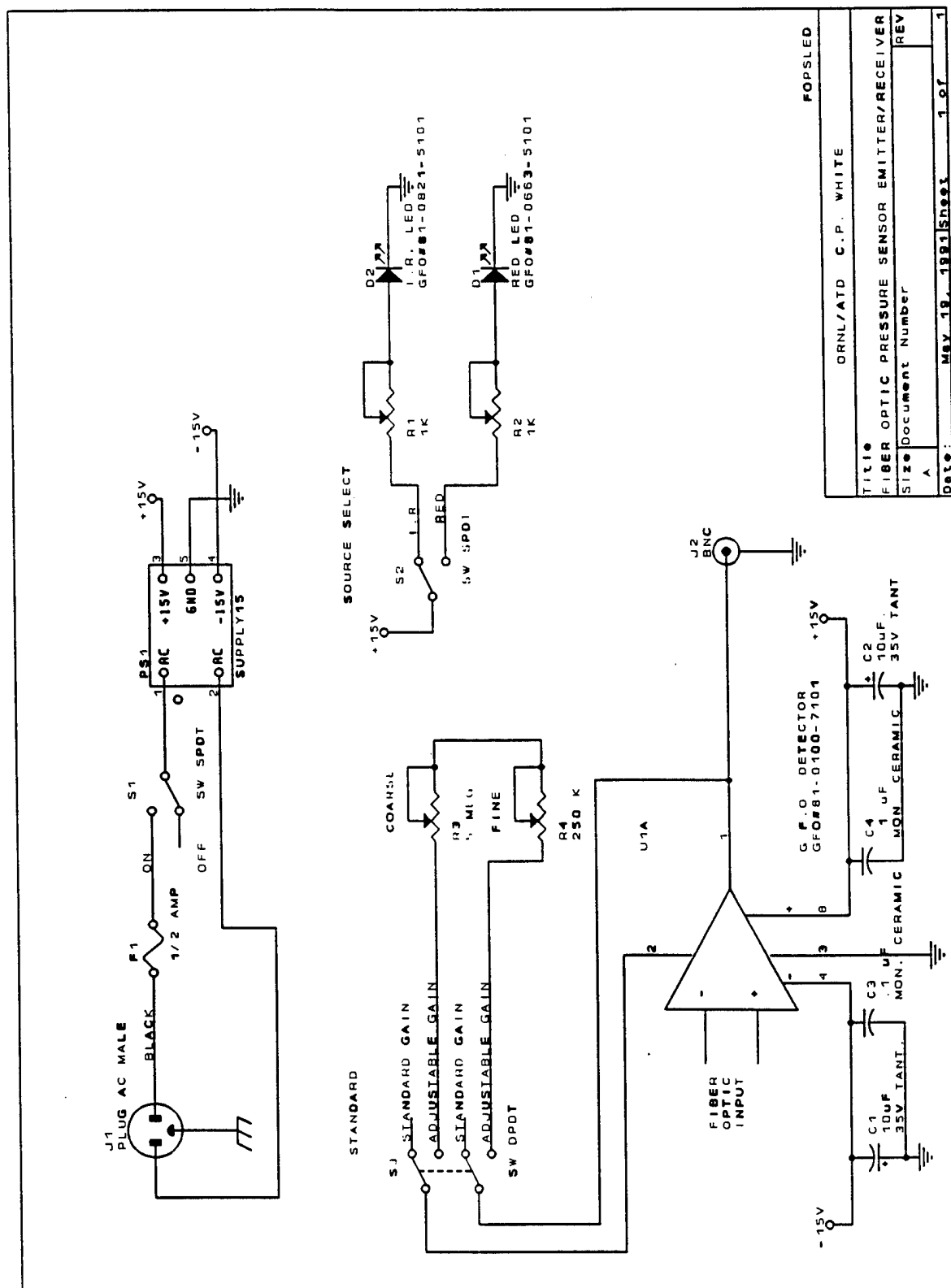


Figure 8. Electronic Schematic of the Opto-Electronic Interface (OEI) Module.

SECTION IV

TESTING OF SELECTED FIBER-OPTIC PRESSURE SENSORS

A. TEST PLAN

The approach is based on the following characteristics which are considered most important as measures of performance: sensitivity, accuracy, frequency response, signal-to-noise ratio, range, and survivability.

To obtain the required data for establishment of these performance parameters for subject sensors requires testing in both static and time-varying pressures. The test procedure, which will be described in greater detail below, consists of:

1. Measuring signal at pressures ranging from essentially ambient to the maximum achievable with the pressure source.
2. Measuring pressure behind shock waves in a shock tube. There is a fair degree of control of this pressure. As will be described subsequently in the shock tube theory section, shock strength is controlled by setting the burst pressure of the compression side, the expansion pressure value, and choice of gases. There will be some uncertainty in registering the exact burst pressure. However, by measuring shock velocity, shock strength is determined.
3. Measuring time response of the signal as the incident shock wave passes by or impinges on the sensor. The frequency of any ringing should be observed.
4. Measuring the value of the signal-to-noise ratio.

The method for acquiring the data is given below, beginning with a description of instrumentation common to both static and dynamic testing followed by details pertinent to each. Data taking and reduction explanations are included.

B. SENSOR INSTRUMENTATION AND DATA PROCESSING METHODS

The sensor instrumentation consists of a FOPS mounted in a shock tube feedthrough, an LED source, a photodiode detector, electrical signal cables, a digital voltmeter, and a digitizing oscilloscope. A block diagram of the arrangement is shown in Figure 7. An OEI interface module, diagrammed in Figure 8, contains two LED sources [visible ($\lambda = 663$ nm) and infrared ($\lambda = 821$ nm)], a photodiode detector, and a linear-gain signal preamplifier. The LED output and photodiode input on the module are coupled to the input and output fibers on the FOPS with standard fiber-optic couplers. The preamplifier output is delivered to the voltmeter or the oscilloscope through a 50-ohm coaxial cable. The voltmeter is used for

static pressure measurements and the oscilloscope is used for shock tube measurements. The voltage of the signal observed is a representation of the optical transmission intensity.

C. STATIC TESTING

During static testing, the increased pressure on the sensor causes either a steady compression of the silicone rubber fiber or a steady shift of the external index of refraction. The result is a steady-state shift in light intensity through the FOPS that can be read directly from the voltmeter. Measurements are obtained by placing the FOPS in a pressure cell and measuring its transmission in the pressure range 100 to 24,500 kPa. The number of calibration points should be sufficient to allow a reliable least-squares fit to the calibration curve. The calibration curve should be displayed as a plot having pressure values on the abscissa axis and normalized transmission values on the ordinate axis. The maximum transmission signal (i.e., the signal measured at 100 kPa pressure) should be normalized to a value of one. A four-way tee fitting may be used as the chamber for the static testing. A FOPS, pressure relief valve, and gauge may be directly attached to each port. The remaining port may connect to the regulator of the compressed gas tank. This method requires only a small amount of gas. The shock tube itself may be used for static calibrations; this expends the gas supply rapidly and is not recommended, especially when using helium.

D. DYNAMIC TESTING

For dynamic testing, the data are recorded in an oscilloscope which is operated in single-shot waveform acquisition mode. The horizontal sweep is typically 200 ms long and the resolution between digitized points is typically 5 μ s. The trigger is adjusted to start on the negative-going edge of the initial pressure pulse. About 20 ms of pretrigger information is recorded on the waveform. Waveforms are usually stored on the disk drive of a laboratory microcomputer by transferring the waveform via an IEEE-488 interface between the two devices. The tests at time-varying pressures are to be performed in a shock tube device. The test pressures should have magnitudes on the order of 24,500 kPa and should have a duration on the order of 1 ms. Since the FOPS exhibit a decrease in transmission signal with increased pressure, the shock-wave pressures are manifested as transient decreases in the FOPS transmission signal.

E. PERFORMANCE COMPARISON

The test results are presented and described in Appendix C. The following is a comparison of sensor results with respect to the measures of performance previously stated.

1. Sensitivity. The SRFOPS and RIFOPS-A exhibited a static pressure sensitivity of 0.07 percent and 0.026 percent

decrease per kPa, respectively. If the slope of the data is extrapolated to where the signal has dropped to 10 percent, the pressures correspond to 15,000 and 50,000 kPa, respectively. This is an indication of their static pressure range for the employed designs. There were flaws in the RIFOPS-B static calibration tests and no reliable sensitivity data were obtained. An earlier version previously reported exhibited a static sensitivity of 0.0001 percent per kPa. By extrapolation, to reduce the signal to the 10 percent level, approximately 900,000 kPa would be required. The dynamic tests of the final RIFOPS-B imply that either its sensitivity is greater or other phenomena, such as physical perturbation of the fiber, are involved. Nonetheless, this is evidence that the specific design features of bend radius, length of stripped fiber, etc., are important in determining the sensitivity.

2. Frequency Response. None of the fiber-optic sensors exhibited discernible ringing. The KPPT sensor (piezo-resistive) ringing frequency for these tests was 5.15 ± 0.14 kHz for a duration of about 1.3 ms. The amplitude of ringing was as much as 50 percent of the mean value of the signal. All the sensors appeared to be able to respond to the initial rise times which were of the order of 100 μ s.
3. Accuracy. A larger database of static testing of the fiber sensors and a statistical analysis would be needed to quantify the accuracy of the sensors for static pressures to be known within 5 percent. Nevertheless, the focus of the present work has been the dynamic application. The results of the KPPT sensor for the initial rise of the pulse were 20 percent smaller than that determined from the shock speed calculations. Because of ringing, the uncertainty of the measurement immediately behind the shock front is greater. The SRFOPS yielded a pressure measurement eight times greater than the calculated value if only the static testing as calibration is assumed. The origin of this eight-fold effective gain increase is not known. It may be due to viscoelastic effects. It is indicative of greater sensitivity to dynamic pressure and, in combination with the low noise characteristics, is evidence of the good potential that may be realized with sufficient dynamic characterization. A modicum of testing would indicate if this gain increase is constant or linear with pressure. Finally, the results were not of sufficient detail to allow a determination of the accuracy of the RIFOPS A and B sensors.
4. Signal-to-Noise Ratio. It appears from comparison of the temporal profile data, that the SRFOPS sensor exhibits a better signal-to-noise ratio than the KPPT sensor. Determination of the RIFOPS A and RIFOPS B noise with respect to the SRFOPS noise from the temporal profile data

in Appendix C is not possible since the random noise levels were too small to allow a comparison.

5. Range and Survivability. The fiber sensors were tested to 6,140 kPa, which was the highest pressure produced in the shock tube tests. The upper limit for shock wave pressure survivability is not known, but is expected to be much higher. All survived the tests.

SECTION V

CONCLUSIONS AND RECOMMENDATIONS

A. CONCLUSIONS

A variety of sensing schemes were evaluated. Three fiber-optic pressure sensor designs were chosen for further design, fabrication, and testing. A significant fraction of the effort was expended in the design and fabrication of a special facility, a shock tube, to produce high-pressure impulses for sensor testing. The sensors were calibrated under static pressure conditions and then tested by measuring pressures in strong shock waves generated in a shock tube. The test results are presented in Appendix C. In the tests, the sensors measured shock waves with peak pressures on the order of 5,000 kPa, pressure rise times on the order of 100 μ s, and flow durations of the pressure spikes of about 200 μ s.

The sensors produced pressure profiles that clearly revealed the temporal structure of the shock waves. The pressure rise in the incident and reflected shock waves was measured at a resolution of approximately 1,000 kPa/ μ s. All three sensors provided a virtually instantaneous response to the steep changes in pressure that were present across the shock front. No periodic ringing was observed in the sensor outputs, in contrast to the ringing observed in the output of a piezoresistive pressure transducer that was also used in the tests. The SRFOPS sensor appeared to be able to follow the pressure profile in the region immediately behind the shock wave in the area where the diaphragm ringing was most severe.

B. RECOMMENDATIONS

The refractive index fiber-optic pressure sensor type A (RIFOPS-A) and the silicone rubber fiber-optic pressure sensor (SRFOPS) are the most promising of the three sensor designs. The SRFOPS has the most immediate potential. In addition to stand-alone operation, it appears possible that, in some situations, these sensors could be operated in a complementary fashion with the conventional diaphragm-type sensors. Since the RIFOPS-A is expected to be used in air, it must be calibrated and tested using high-pressure air. At present, the sensors are hand crafted and must be characterized individually to further assess the repeatability, accuracy, and

capability of the sensors. Tests at higher pressures than could be achieved with the compressed gas sources used in the present work would be useful. The shock tube is designed to generate shock waves with pressures as large as 24,500 kPa, and these shock waves can be achieved by using a compressor to pressurize the compression chamber.

A final recommendation concerns sensor mounting. It is important to securely hold the fiber(s) in an immobile position to prevent their shaking during the shock tube gas flow.

REFERENCES

1. Allison, S. W., Dynamic High-Pressure Measurement Using Optical Fiber Methods, Oak Ridge National Laboratory, Oak Ridge, TN, Report EPD-2, December 1987.
2. Allison, S. W. et al., "Fiber-Optic Schemes for Fast-Response Pressure Sensing," Proceedings of the SPIE Conference on High Bandwidth Analog Applications of Photonics II, Vol. 987, pp. 20-28, Boston, MA, September 8-9, 1988 (SPIE, Bellingham, WA, 1989).
3. Wright, J. K., Shock Tubes, p. 40, John Wiley, New York, NY, 1961.
4. Yeh, C., Handbook of Fiber Optics, p. 14, Academic Press, San Diego, CA, 1990.
5. Krohn, D. A., Fiber Optic Sensors: Fundamentals and Applications, p. 32, Instrument Society of America, Research Triangle Park, NC, 1988.
6. Krohn, p. 136-138.

APPENDIX A

THE SHOCK TUBE

A. SHOCK TUBE DESCRIPTION AND DESIGN CONSIDERATIONS

A shock tube is a relatively simple device that can produce controlled shock waves. Many of the physical properties of these waves, such as shock strength and gas flow velocity, can be calculated analytically; this makes the shock tube a useful instrument for testing sensors designed to measure pressures in transient, high-pressure waves. For this reason, a shock tube capable of producing shock waves with pressures comparable to those produced by a 900-kg bomb was designed and constructed as part of this work.

A shock tube consists of a rigid cylinder, closed at the ends, and divided into two interior chambers by a gas-tight diaphragm mounted normal to the cylinder axis (see Figure A-1). A pressure difference is applied across the diaphragm by filling the compression chamber with a gas at high pressure and maintaining the expansion chamber at low pressure. At a sufficiently large pressure difference, the diaphragm ruptures, and the pressures in the tube equalize by a shock wave that propagates into the expansion chamber and a rarefaction wave that propagates into the compression chamber. When the expansion chamber possesses a constant cross-sectional area, the pressure and particle velocity remain constant over a certain region behind the shock wave. When the shock wave reaches the rigid wall at the end of the expansion chamber, it undergoes a reflection and reverses its direction of travel. When the shock front on the reflected wave meets the high-temperature gas behind the shock front, a further increase in pressure occurs at the shock front. The pressure in the reflected shock wave can sometimes be considerably larger than that in the incident wave.

The following is a brief description of the shock tube used in this work. (The tube layout is shown in Figure A-2.) The compression chamber is 1.2 meters long, and the expansion chamber is 3.8 meters long. Both chambers have an inside diameter of 7.6 cm. The diameter of the flange aperture is also 7.6 cm. The flow of gas to and from the tube is controlled from a gas-handling manifold, and high-pressure hoses connect the manifold valves to the two chambers in the tube. Mounted on the manifold are general-purpose dial pressure gauges (Omega Models PGS-35B-600 and PGS-35B-10000) that are used to monitor the pressures in the chambers. The accuracy of the gauges is specified as ± 1 percent of their full-scale reading (± 690 kPa for the gauge reading the compression chamber pressure and ± 40 kPa for the gauge reading the expansion chamber pressure).

PRESSURE WAVES IN A SHOCK TUBE

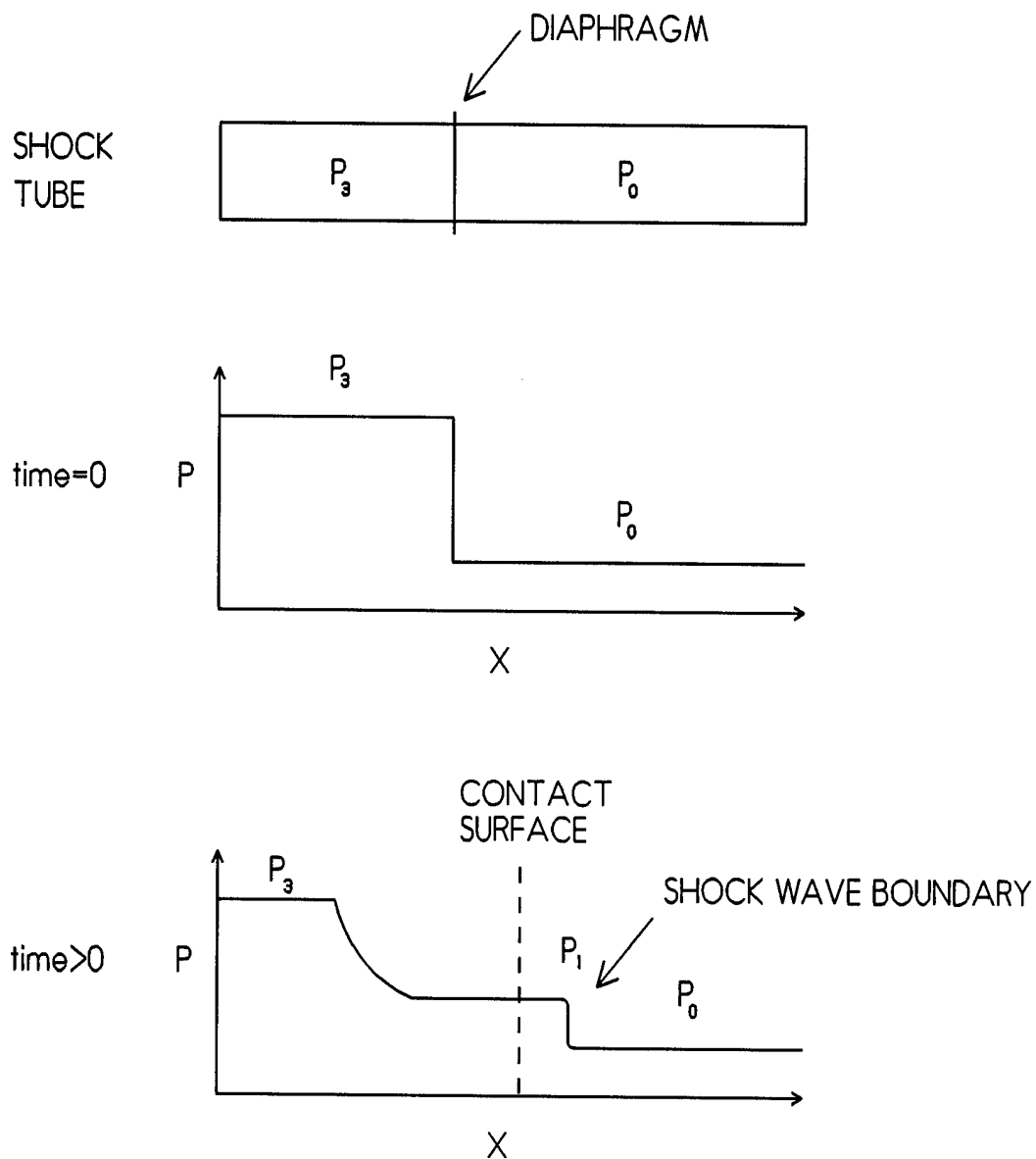


Figure A-1. Illustration of Shock Tube Pressure Profiles before (Time = 0) and after (Time > 0) the Rupture of the Diaphragm.

SHOCK TUBE LAYOUT

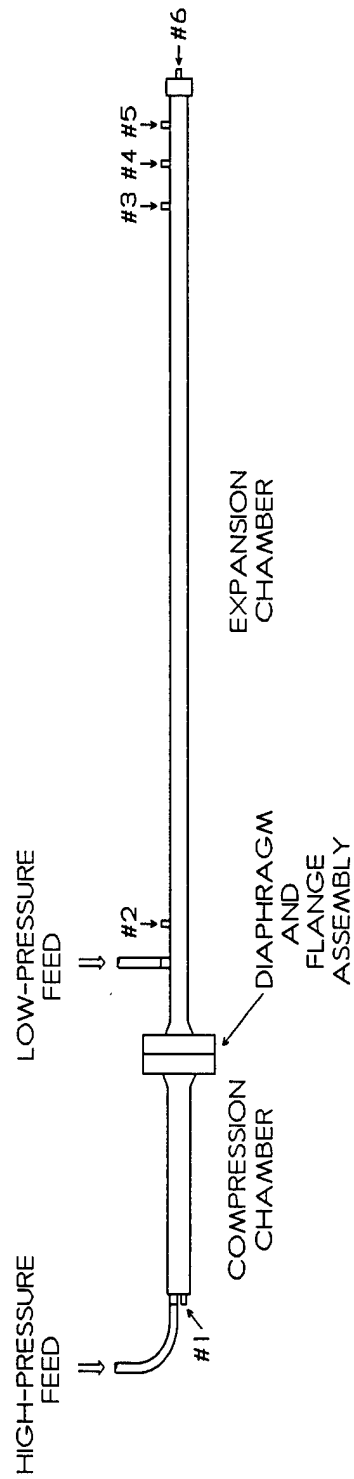


Figure A-2. Shock Tube Layout, Showing Positions of Instrumentation Ports 1-6.

Six instrumentation ports are present on the shock tube. These ports allow pressures inside the tube to be monitored by pressure sensors or regulated by pressure relief valves. Port 1 is located on the end wall of the compression chamber, Ports 2 through 5 are located on the top of the expansion chamber, and Port 6 is located on the end wall of the expansion chamber. Table A-1 lists the distances of the ports from the plane of the diaphragm.

TABLE A-1. SHOCK TUBE DIAPHRAGM-TO-PORT DISTANCES

Port	Distance (cm)
1	120
2	51
3	332
4	347
5	362
6	380

The flange assembly accepts rupture disks (nickel metal, size 3"H, type SPL B) manufactured by BS&B Safety Systems of Tulsa, Oklahoma. The disks are designed to rupture at specific pressures and are scored at the center so they "petal open" rather than shatter.

Shock tubes and high-pressure equipment are in widespread industrial use, and the associated hazards are considered to be standard industrial hazards. Standard safety practices and engineering and administrative controls are sufficient to prevent mishaps and other injuries. Engineering controls include the use of restraints for compressed gas cylinders, failsafe pressure relief devices, and equipment rated for use at the maximum working pressure. Administrative controls include the implementation of periodic equipment inspections and a requirement that the shock tube be operated from a shielded, remote location.

B. SHOCK TUBE PARAMETERS

A brief discussion of the properties of shock waves produced in shock tubes is given here. The reader is directed to References A-1 and A-2 for a complete discussion of shock tube dynamics and a derivation of the equations.

The essential shock wave properties can be calculated from a few equations. The basic shock tube parameter is the shock strength, given by

$$Y = p_1/p_0 , \quad (A-1)$$

where p_0 is the initial pressure in the expansion chamber and p_1 is the pressure behind the shock wave. The shock strength is obtained by solving the shock tube equation

$$\frac{c_0}{c_3} \frac{(1-\mu_0)(y-1)}{\sqrt{[(1+\mu_0)(y+\mu_0)]}} = \frac{2}{(\gamma_3-1)} \left[1 - \left(\frac{p_0}{p_3} y \right)^\beta \right] , \quad (A-2)$$

where

p_3 is the initial pressure in the compression chamber, γ_0 and γ_3 are the heat capacity ratios (i.e., heat capacity at constant pressure divided by heat capacity at constant volume),

$$\mu_0 = (\gamma_0-1)/(\gamma_0+1) ,$$

$$\beta = (\gamma_3-1)/2\gamma_3 , \text{ and}$$

c_0 and c_3 are the acoustic velocities.

Acoustic velocities are obtained from the Lagrangian formula

$$c = (\gamma RT/MW)^{1/2} , \quad (A-3)$$

where R is the universal gas constant ($8314.3 \text{ J} \cdot \text{kmole}^{-1} \cdot \text{K}^{-1}$), T is the absolute temperature, and MW is the molecular weight. Table A-2 lists values of MW and γ for various gases.

TABLE A-2. VALUES OF MW AND γ FOR VARIOUS GASES.

Gas	MW (kg/kmole)	γ
air	28.934	1.40
N_2	28	1.40
He	4	1.66
Ne	20	1.64
Ar	40	1.67

When y has been obtained from the solution of Equation (A-2), the velocity U of the shock front can be calculated from

$$U = c_0 M = c_0 \sqrt{\frac{y+\mu_0}{1+\mu_0}} , \quad (A-4)$$

where M is the shock Mach number. The shock wave flow velocity u_1 can be calculated from

$$u_1 = c_0 \frac{(1-\mu_0)(y-1)}{\sqrt{[(1+\mu_0)((y+\mu_0))]} . \quad (A-5)$$

The pressure p_1' of the shock wave after it is reflected by the rigid wall at the end of the expansion chamber is given by

$$p_1' = y p_0 \frac{(2\mu_0+1)y-\mu_0}{\mu_0 y+1} . \quad (A-6)$$

Note that for very strong shock waves ($y \gg 1$), the pressure in the reflected wave approaches the asymptotic value $2+1/\mu_0$. For air ($\mu_0 = 1/6$), this value is 8.

Equations (A-1) through (A-6) have been used in Appendix C to obtain calculated values of the properties of shock waves generated in the shock tube. A computer program that calculates these properties is listed below in Appendix B.

APPENDIX B

COMPUTER PROGRAM FOR CALCULATING PROPERTIES OF SHOCK WAVES

The following is an annotated listing of a MathCAD[®] (MathSoft, Inc., Cambridge, MA) program that calculates the properties of shock waves generated in the shock tube.

SHOCK.MCD - Calculation of shock wave properties using formulas given in J. K. Wright, Shock Tubes, New York, John Wiley, 1961.
D. B. Smith, ORNL/ATD, November 1990

Define shock tube parameters (0 and 3 designate expansion chamber and compression chamber, respectively)

heat capacity ratios	g0 := 1.40 (air)		
	g3 := 1.66 (He)		
initial pressures	p0 := 15·psia	p0 = 103.4·kPa	
	p3 := 815·psia	p3 = 5619·kPa	
initial temperatures	T0 := 293·K		
	T3 := T0		
molecular weights of gases	MW0 := 28.934· $\frac{\text{kg}}{\text{kmole}}$	MW3 := 4· $\frac{\text{kg}}{\text{kmole}}$	
universal gas constant	R := 8314.3· $\frac{\text{J}}{\text{kmole} \cdot \text{K}}$		
acoustic velocities	c0 := $\sqrt{\frac{g0 \cdot R \cdot T0}{MW0}}$	c3 := $\sqrt{\frac{g3 \cdot R \cdot T3}{MW3}}$	

Solve for shock strength y (Wright Eq. 3.1)

$$\mu_0 := \frac{g_0 - 1}{g_0 + 1} \quad \beta := \frac{g_3 - 1}{2 \cdot g_3}$$

$$f(y) := \text{root} \left[\left[\frac{c_0}{c_3} \right] \cdot \left[\frac{(1 - \mu_0) \cdot (y - 1)}{\sqrt{(1 + \mu_0) \cdot (y + \mu_0)}} \right] - \left[\frac{2}{g_3 - 1} \right] \cdot \left[1 - \left[\frac{p_0}{p_3} \right] \cdot y \right]^\beta, y \right]$$

Initial guess for y y := 11

Solution for y y := f(y)
y = 11.432

Calculate pressure behind shock wave

$$p_1 := y \cdot p_0 \quad (\text{Wright, Eq. 2.24})$$

$$p_1 = 1.182 \cdot 10^3 \cdot \text{kPa} \quad p_1 = 171.485 \cdot \text{psia}$$

Calculate velocity of shock front

$$M := \sqrt{\frac{y + \mu_0}{1 + \mu_0}} \quad \text{shock Mach number}$$

$$U := c_0 \cdot M$$

$$U = 1.083 \cdot 10^3 \frac{\text{m}}{\text{s}}$$

Calculate flow velocity behind shock wave

$$u_1 := c_0 \cdot \frac{(1 - \mu_0) \cdot (y - 1)}{\sqrt{(1 + \mu_0) \cdot (y + \mu_0)}} \quad (\text{Wright, p. 32})$$

$$u_1 = 811.378 \frac{\text{m}}{\text{s}}$$

Calculate pressure behind reflected shock wave

$$p_{1r} := \left[\frac{(2 \cdot \mu_0 + 1) \cdot y - \mu_0}{\mu_0 \cdot y + 1} \right] \cdot p_1 \quad (\text{Wright, Eq. 6.5})$$

$$p_{1r} = 6.136 \cdot 10^3 \cdot \text{kPa} \quad p_{1r} = 889.86 \cdot \text{psia}$$

Unit definitions (SI system)

$\text{kg} \equiv 1\text{M}$	$\text{m} \equiv 1\text{L}$	$\text{s} \equiv 1\text{T}$
$\text{N} \equiv \text{kg} \cdot \frac{\text{m}}{\text{s}^2}$	$\text{kPa} \equiv 10^3 \cdot \frac{\text{N}}{\text{m}^2}$	$\text{psia} \equiv 6.895 \cdot \text{kPa}$
$\text{K} \equiv 1$	$\text{kmole} \equiv 1$	$\text{J} \equiv \text{N} \cdot \text{m}$

APPENDIX C

TEST RESULTS

A. STATIC PRESSURE CALIBRATION TESTS

The FOPS described in Section II were evaluated by the measures of performance given in Section IV. Section IV outlines the procedures for tests at static and time-varying pressures, the method for sensor data acquisition, and the method for data analysis. Static pressure tests provide sensor calibration data, while tests at time-varying pressures provide data used to determine the accuracies and temporal response characteristics of the sensors. The results of the evaluation are presented below.

The calibration of a FOPS involves a measurement of its optical transmission at known values of static pressure. The FOPS are designed to exhibit a decrease in transmission with increasing pressure. Figures C-1(a) and C-1(b) show static calibration curves for the refractive-index sensor type A (RIFOPS-A) and the microbend-loss sensor (SRFOPS), respectively. The transmission is shown on the vertical scale as normalized signal, where the signal at atmospheric pressure is defined to be equal to one. Nitrogen gas (N_2) was used for these calibration measurements, and the pressure values were read from a pressure gauge having an uncertainty of ± 40 kPa.

A linear least-squares fit was performed for the static calibration curve of each FOPS. These fits are shown as solid lines in the figures. Expressions for static pressure as a function of normalized sensor signal were derived from the coefficients of the fit and are also shown in the figures. For the transient high-pressure tests (Section B below), fits such as these were used to convert the FOPS signals into pressure values.

The percent decrease in transmission signal per unit pressure increase is a measure of the pressure sensitivity of each FOPS. The sensor sensitivities [obtained from the static calibration data shown in Figures C-1(a) and C-1(b)] are compared in Table C-1. Note that the SRFOPS is approximately 2.7 times more sensitive than the RIFOPS-A.

TABLE C-1. FOPS SENSITIVITY COMPARISON

Sensor Design	Pressure Sensitivity (% decrease in transmission per kPa)
RIFOPS-A	0.026
SRFOPS	0.070

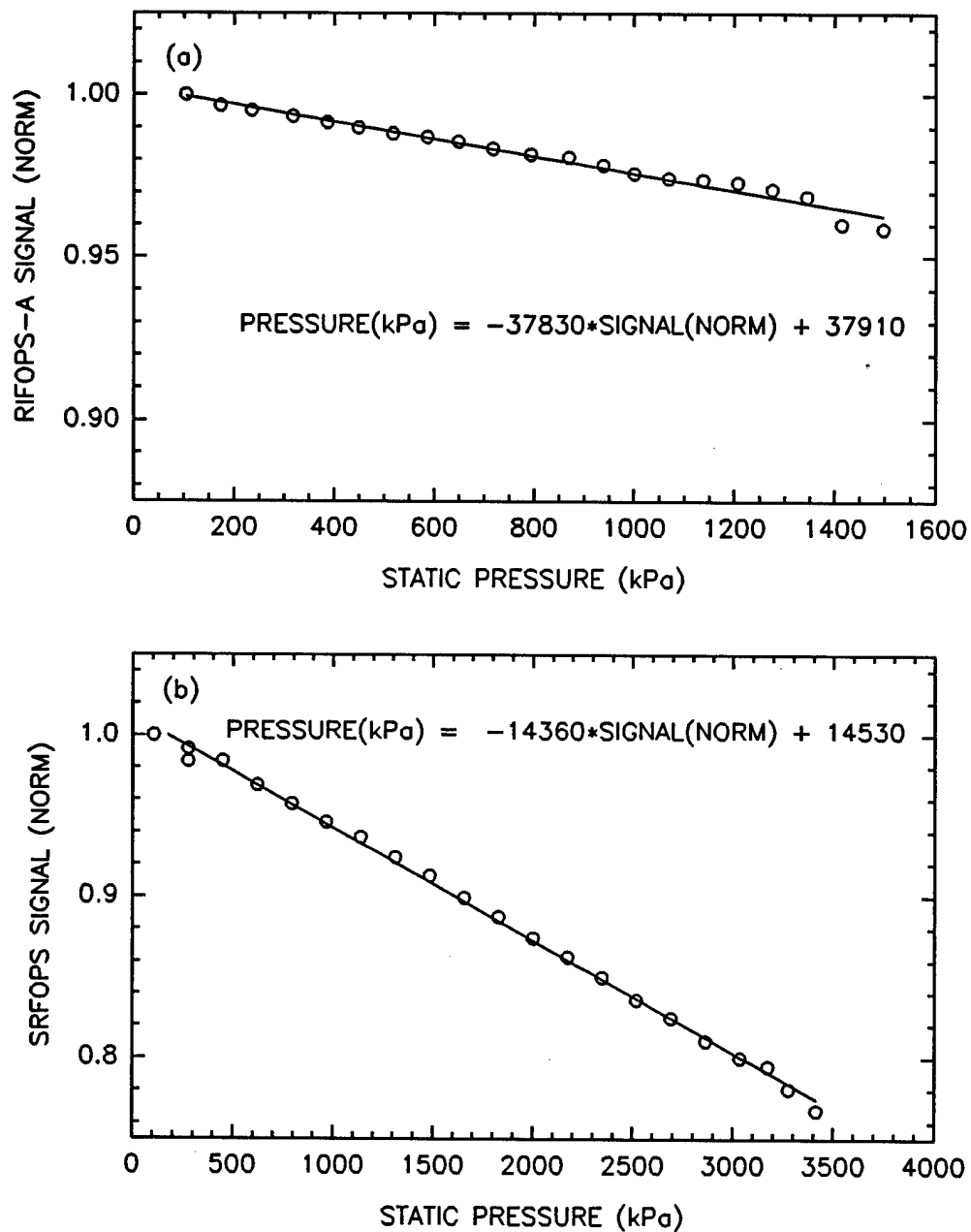


Figure C-1. Calibration of (a) RIFOPS Type A and (b) SRFOPS using Static Pressures of N_2 . The solid lines are linear least-squares fits to the data, and the equations are derived from the fits.

B. DYNAMIC PRESSURE CALIBRATION TESTS

The dynamic pressure calibrations were done using a shock tube designed specifically for this study. A description of the shock tube and its design parameters is given in Appendix A, and instructions for its use are given in Reference C-1.

The shock tube tests were performed with high-pressure He or N₂ gas in the compression chamber and air at atmospheric pressure (103 kPa) in the expansion chamber. The He and N₂ were obtained from 6,000-liter compressed gas cylinders (14,000 kPa maximum pressure). Sheets of 0.13-mm-thick stainless steel or brass were usually used as inexpensive diaphragms, but a few tests were performed with BS&B diaphragms designed to rupture at a pressure difference of 7,420 kPa. The brass and stainless steel diaphragms ruptured at pressure differences that varied from 4,800 to 5,500 kPa.

A piezoresistive pressure transducer, Kulite Semiconductor Model HKS-375-5000 SG (KPPT), was used in several of the shock tests, and, whenever possible, its output was compared to the FOPS signals. This pressure transducer, henceforth referred to as the KPPT, has a sensitivity of 3.6 μ V per kPa over the pressure range 100 to 35,000 kPa. Pressures are determined from the expression

$$P(\text{kPa}) = (2.8 \times 10^5 \text{ kPa/V}) [S_{\text{KPPT}}(\text{V}) \pm S_{\text{KPPT},0}(\text{V})] , \quad (\text{C-1})$$

where S_{KPPT} is the pressure signal and $S_{\text{KPPT},0}$ is the zero pressure signal. The uncertainty of the signal is ± 0.5 percent.

1. Silicone Rubber Fiber-Optic Pressure Sensor (SRFOPS)

Temporal profiles of the signals produced by the SRFOPS and the KPPT when exposed to a shock wave are shown in Figure C-2(a) and Figure C-2(b). The shock wave was generated by the expansion of high-pressure ($5,620 \pm 345$ kPa) helium in the compression chamber into the low-pressure (103 kPa) air in the expansion chamber. The signals were acquired simultaneously, and the horizontal axis indicates the time elapsed from when the oscilloscope was triggered by the first pulse in the SRFOPS profile. The SRFOPS was mounted in Port 3 of the shock tube and the KPPT was mounted in Port 6. This arrangement allowed the SRFOPS to measure the pressure profile of the shock wave before and after reflection from the end of the expansion chamber and allowed the KPPT to measure the pressure profile of the shock wave during its reflection from the end of the chamber.

The first pulse in the SRFOPS profile (indicated by 1) is the incident shock wave, and the second pulse (indicated by 1') is the reflected shock wave. Four sets of incident and reflected shock waves are observable in the profile. The four pulses in the KPPT profile (indicated by 1-4) were produced as the shock wave underwent reflection at the end of the expansion chamber. The

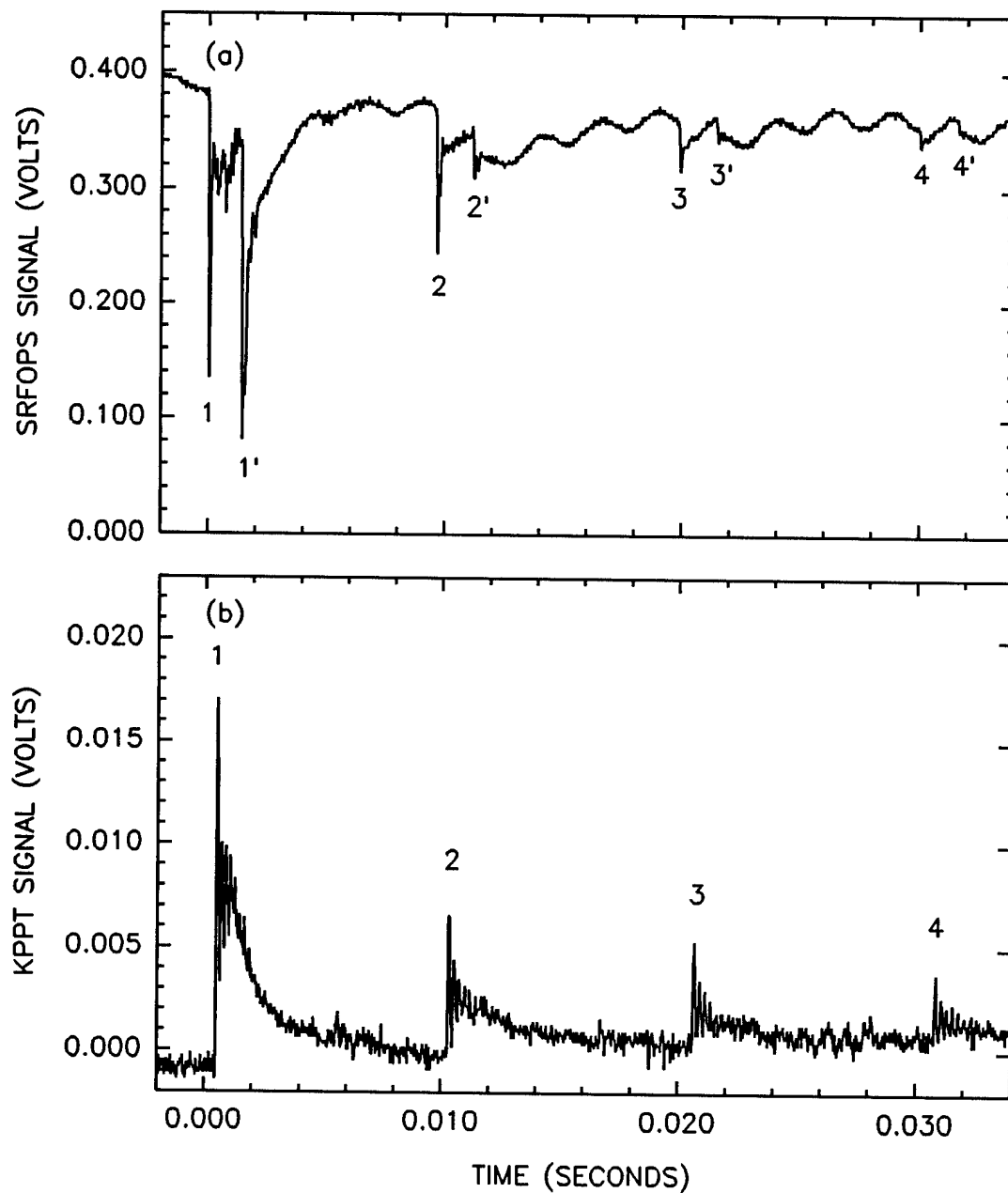


Figure C-2. Temporal Profiles of the Signals Produced by (a) the SRFOPS and (b) the KPPT in Response to a Shock Wave.

pulses occurred in both profiles at approximately 10-ms intervals, and their presence indicates that the initial shock wave probably underwent successive reflections from the diaphragm or the contact discontinuity in the expansion chamber. [The contact discontinuity marks the boundary between the gases that were initially on opposite sides of the diaphragm (Reference C-2).] Reflected waves were observed in all of the shock tube tests.

A 400-Hz sinusoidal oscillation with a peak-to-peak magnitude of approximately 0.3 volts is observable in the SRFOPS profile. This signal is an artifact of the recoil and subsequent vibration of the shock tube after the rupture of the diaphragm and is not attributable to pressure variations at the SRFOPS.

Time-expanded views of the initial shock wave are shown in Figures C-3(a) and C-3(b). The SRFOPS pulse corresponding to the incident shock wave (indicated by 1) has a rise time of 70 μ s, and its width indicates that the duration of gas flow was about 200 μ s. The SRFOPS pulse corresponding to the reflected shock wave (indicated by 1') also has a rise time of 70 μ s. The small pulses between pulses 1 and 1' and after pulse 1' are aperiodic and are not an indication of ringing by the sensor. These pulses could be an indication of turbulent flow behind the shock wave.

The KPPT pulse, which corresponds to the reflection of the incident shock wave, has a rise time of 50 μ s. In contrast to the SRFOPS signal profile, the KPPT signal profile is characterized by oscillatory ringing. The ringing frequency is 5.15 ± 0.14 kHz, and it was present for approximately 1.3 ms.

The SRFOPS and the KPPT shock wave pressure profiles are shown in Figures C-4(a) and C-4(b). The SRFOPS signal was converted to pressure values using the calibration equation shown in Figure C-1(b), and the KPPT signal was converted to pressure values using Equation (C-1). The pressures measured by the sensors can be compared with the values calculated from Equations (A-1), (A-2), and (A-6). We have

$$p_1 = (11.4 \pm 0.3) (103 \text{ kPa}) = 1180 \pm 30 \text{ kPa} \quad (\text{C-2})$$

and

$$p_1' = (11.4 \pm 0.3) (103 \text{ kPa}) \frac{[(2) (1/6) + (11.4 \pm 0.3)] - (1/6)}{(1/6) (11.4 \pm 0.3) + 1} \quad (\text{C-3})$$

$$= 6140 \pm 610 \text{ kPa}$$

(The uncertainties in the calculated values of p_1 and p_1' are due to the uncertainty in p_0 .) Figure C-1(a) shows that the SRFOPS measured the pressure of the incident wave as 9,400 kPa, a value eight times larger than the calculated value if the static calibration is assumed. This is surprising in view of how well the

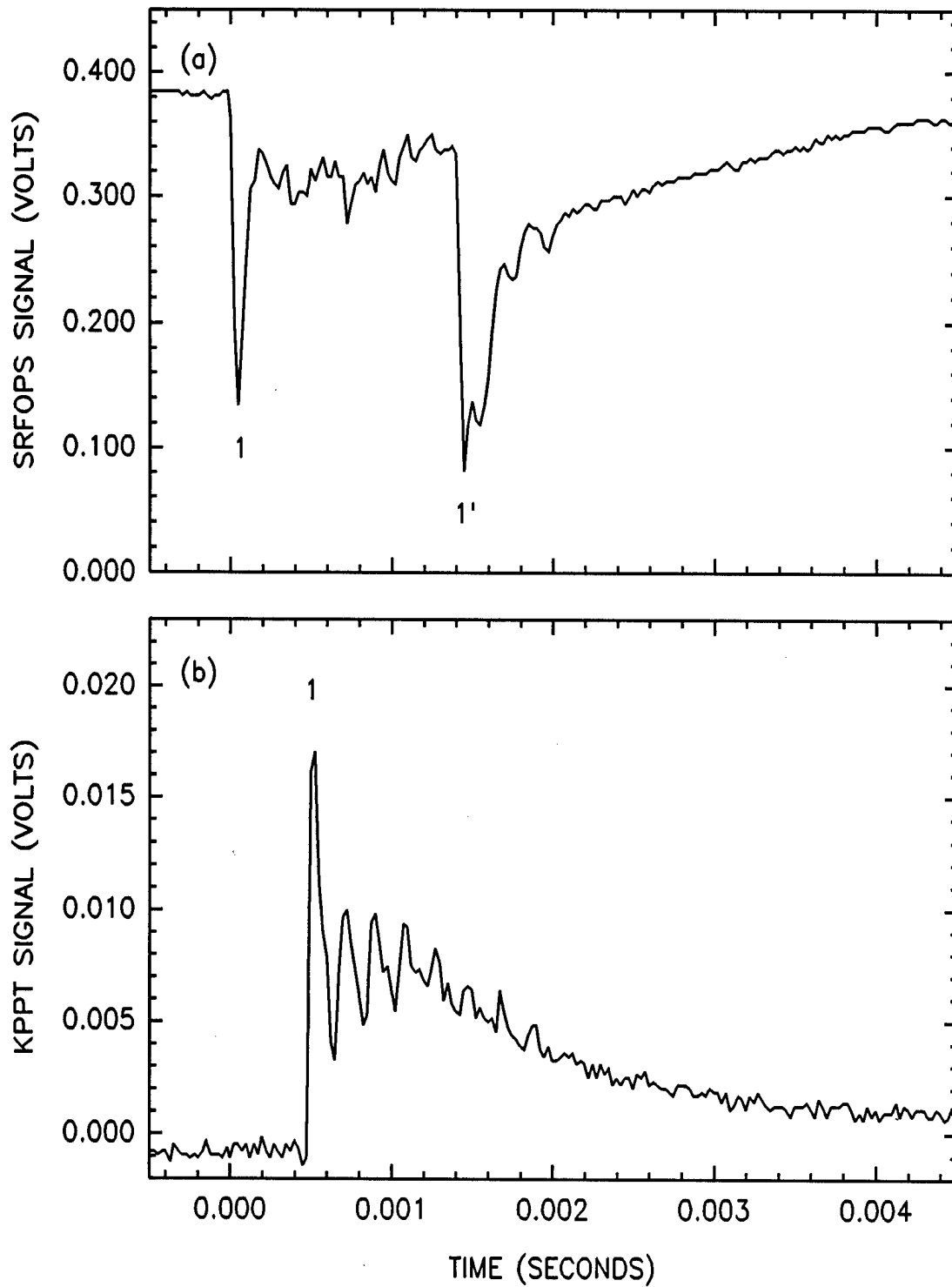


Figure C-3. Expanded Views of the First Shock Wave Pulses Shown in Figures C-2(a) and C-2(b).

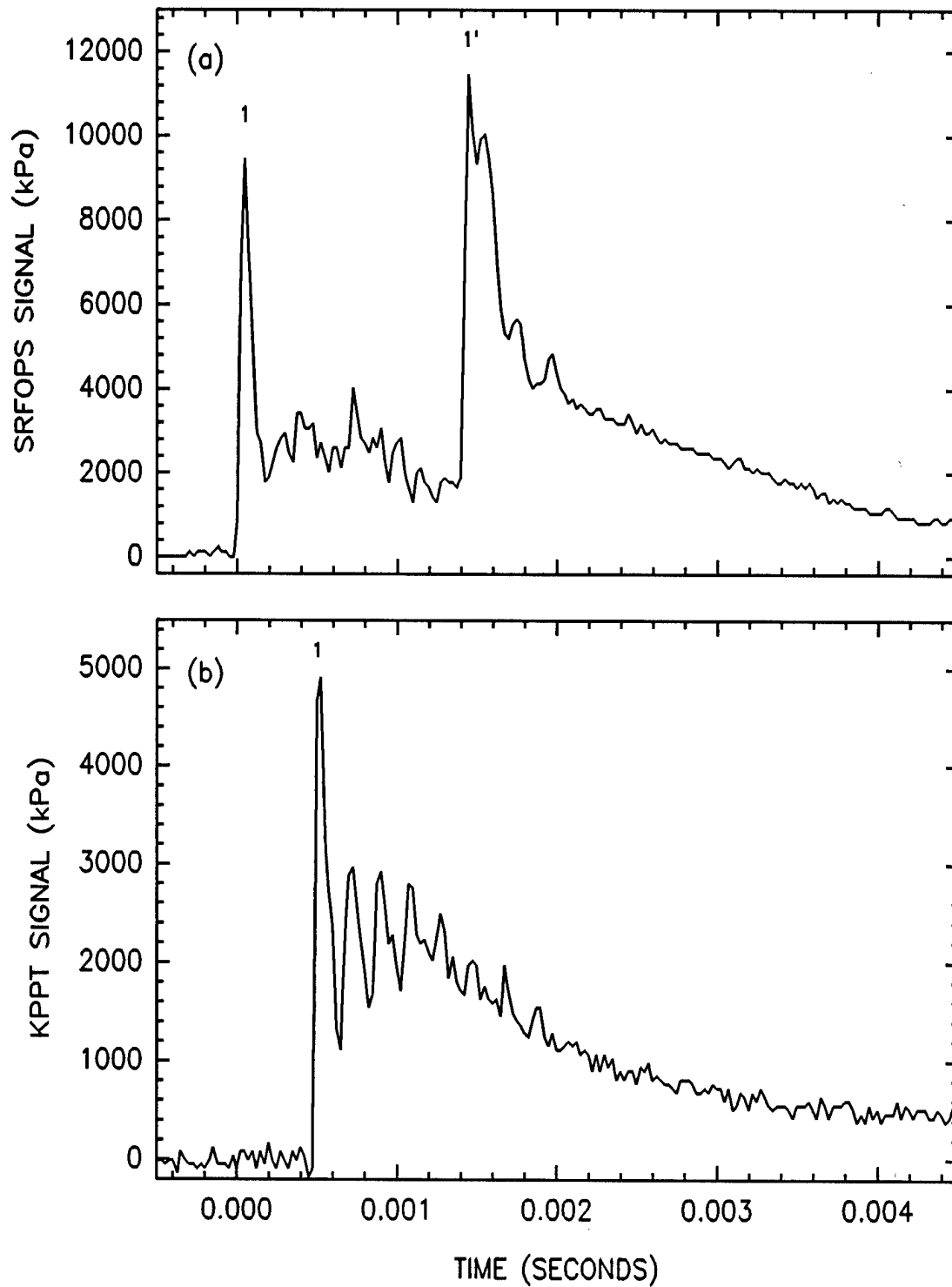


Figure C-4. Shock Wave Profiles Shown in Figures C-3(a) and C-3(b) after Conversion into Pressure Units.

quality of the SRFOPS data appear in comparison to the KPPT results. In Figure C-1(b) we see that the KPPT measured the pressure of the reflected wave as 4,900 kPa, a value 20 percent smaller than the calculated value.

The shock front velocity can be calculated from Equation (A-4). We have

$$U = (343 \text{ m/s}) \left[\frac{(11.4 \pm 0.3) + (1/6)}{1 + (1/6)} \right]^{1/2} = 1080 \pm 14 \text{ m/s} . \quad (\text{C-4})$$

The measured value of U is obtained by dividing the distance between Ports 3 and 6 (48 cm) by the time elapsed between the onsets of the SRFOPS and KPPT signals. We have

$$U = (0.48 \text{ m}) / (500 \times 10^{-6} \text{ s}) = 960 \text{ m/s} . \quad (\text{C-5})$$

The measured value of U is 11 percent smaller than the calculated value.

2. Refractive-Index Fiber-Optic Pressure Sensor Type A (RIFOPS-A)

Temporal profiles of the signals produced by the SRFOPS and the RIFOPS-A are shown in Figure C-5(a) and Figure C-5(b), respectively. The figures show only the first shock wave pulse in the acquired waveform. The shock wave was generated by the expansion of high-pressure ($4,420 \pm 345 \text{ kPa}$) helium in the compression chamber into the low-pressure (103 kPa) air in the expansion chamber. The SRFOPS was mounted in Port 3 and the RIFOPS-A was mounted in Port 6, so the SRFOPS measured the pressure profile of the incident shock wave before and after reflection from the end of the expansion chamber, and the RIFOPS-A measured the pressure profile of the shock wave during its reflection from the end of the chamber.

The features of the SRFOPS profile are similar to those of Figure C-3 and will not be discussed. The RIFOPS-A profile, however, contains some notable features. The large positive-going pulse (indicated by the arrow) is preceded by a small negative-going pulse (indicated by 1). The small pulse was probably produced by the shock front, which contains the expansion chamber gas (air) on its leading edge, while the large pulse was probably produced by the gas behind the shock front, which contains the compression chamber gas (helium). The small pulse is the result of a decrease in transmission and correlates with the high pressure in the reflected shock wave. On the other hand, the large pulse represents an increase in transmission that can be explained by the presence of the helium. Helium has a much smaller value for n than does air (see Table 1), and the large pulse correlates to the rapid decrease in n_{clad} that occurs when the mixture of helium and air meets the sensing region.

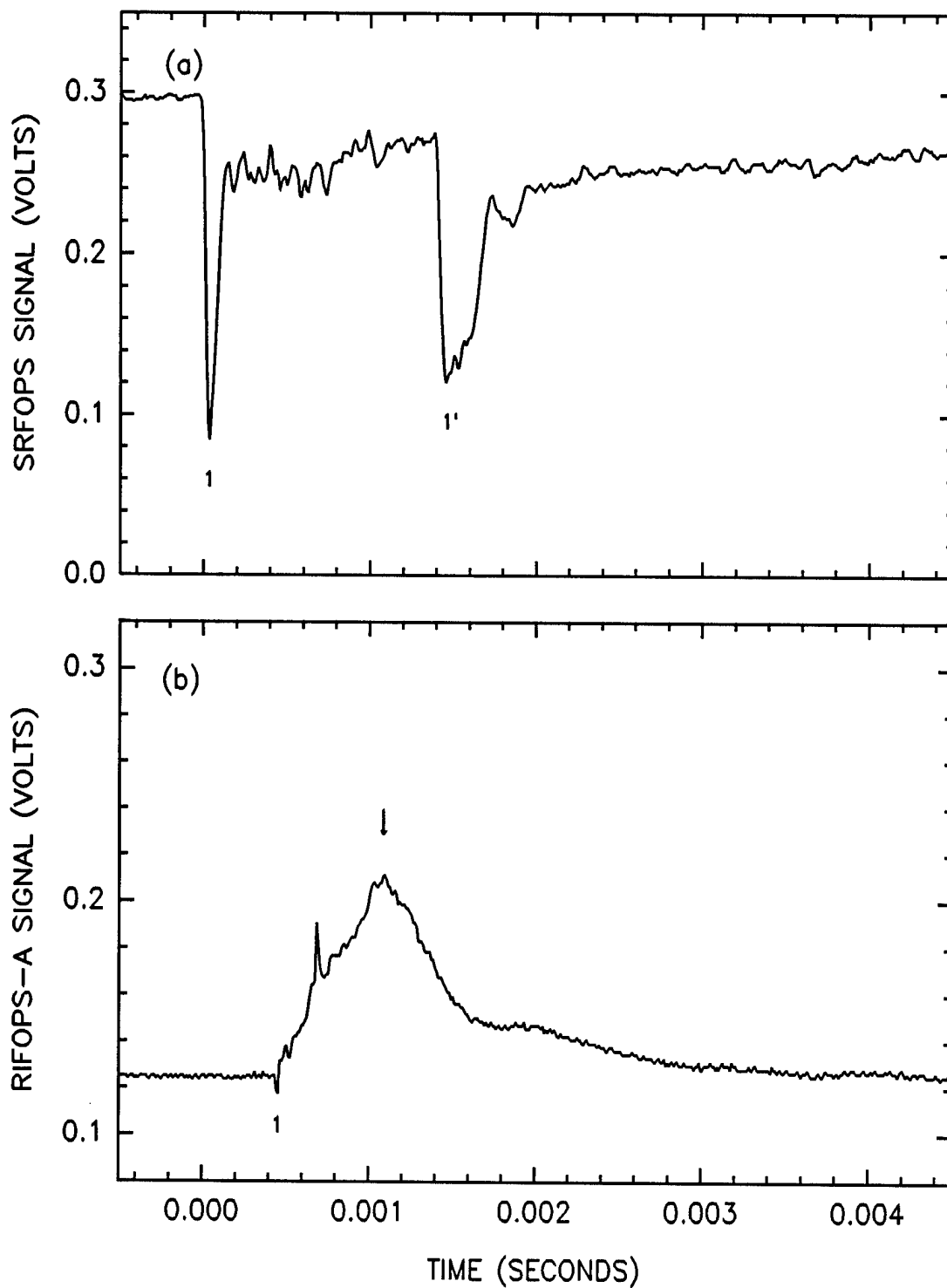


Figure C-5. Temporal Profiles of the Signals Produced by (a) the SRFOPS and (b) the RIFOPS Type A.

Since the RIFOPS-A was not calibrated for a mixture of helium and air (and since it would be very difficult to assess the effect of the mixture flow rate), no pressure profile for the RIFOPS-A was calculated. However, the measured and calculated values for the shock front velocity can be compared. The measured value of U is

$$U = (0.48 \text{ m}) / (455 \times 10^{-6} \text{ s}) = 1060 \text{ m/s} , \quad (\text{C-6})$$

while from Equation (A-4) we have

$$U = 1020 \pm 13 \text{ m/s} . \quad (\text{C-7})$$

The measured and calculated values of U agree within 4 percent.

3. Refractive-Index Fiber-Optic Pressure Sensor Type B (RIFOPS-B)

Temporal profiles of the signals produced by the SRFOPS and the RIFOPS-B are shown in Figures C-6(a) and C-6(b), respectively. The figures show only the first shock wave pulse in the acquired waveform. The shock wave was generated by the expansion of high-pressure ($4,740 \pm 345 \text{ kPa}$) nitrogen (N_2) in the compression chamber into the low-pressure (103 kPa) air in the expansion chamber. The SRFOPS was mounted in Port 3 and the RIFOPS-B was mounted in Port 6, so the SRFOPS measured the pressure profile of the incident shock wave before and after reflection from the end of the expansion chamber, and the RIFOPS-B measured the pressure profile of the shock wave during its reflection from the end of the chamber.

The features of the SRFOPS profile are similar to those of Figure C-3 and will not be discussed. The features in the RIFOPS-B profile are similar to those in the RIFOPS-A profile, which was discussed in the above section. Again, the small negative-going pulse (indicated by 1) was probably produced by the shock front, which contains the expansion chamber gas (air) on its leading edge, while the large positive-going pulse (indicated by the arrow) might have been produced by the heated nitrogen gas behind the shock front.

The measured and calculated values for the shock front velocity can be compared. The measured value of U is

$$U = (0.48 \text{ m}) / (670 \times 10^{-6} \text{ s}) = 720 \text{ m/s} , \quad (\text{C-8})$$

while from Equation (A-4) we have

$$U = 727 \pm 9 \text{ m/s} . \quad (\text{C-9})$$

The measured and calculated values of U agree within the uncertainty of the calculated value.

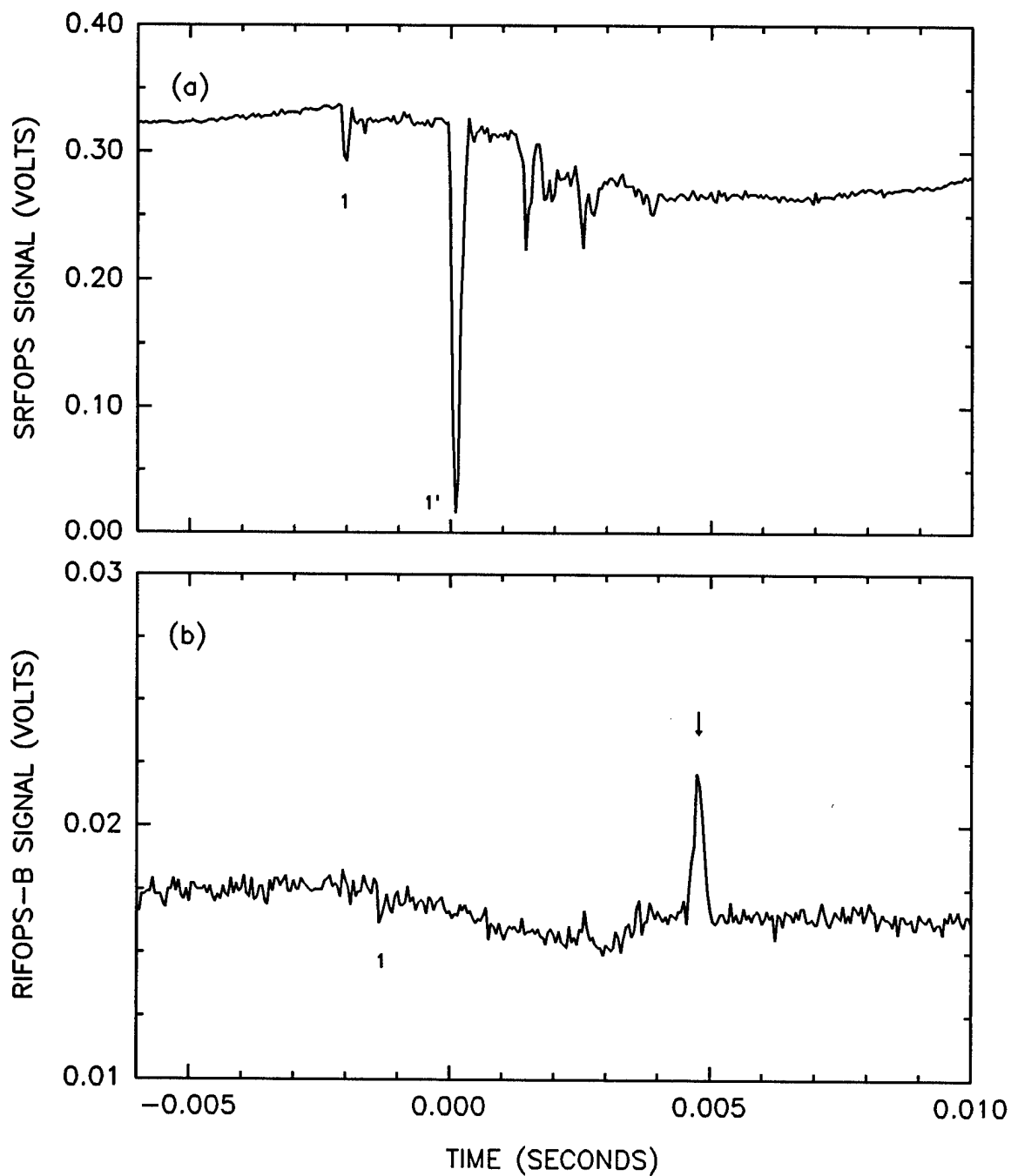


Figure C-6. Temporal Profiles of the Signals Produced by (a) the SRFOPS and (b) the RIFOPS Type B.

REFERENCES

- A-1. Wright, J. K., Shock Tubes, p. 40, John Wiley, New York, NY, 1961.
- A-2. Liepmann, H. W. and A. Roshko, Elements of Gas Dynamics, pp. 79-83, John Wiley, New York, NY, 1957.
- C-1. Smith, D. B., S. W. Allison, J. R. Muhs, and B. L. Johnson, Sr., Operation, Maintenance, and Safety Manual for A Shock Tube Pressure Calibration Facility, ESL-TR-91-25, Engineering and Services Laboratory, Headquarters Air Force Engineering and Services Center, Tyndall AFB, FL, May 1991.
- C-2. Wright, pp. 30, 31.